

# A search for ionised gas outflows in an H $\alpha$ imaging atlas of nearby LINERs <sup>★</sup>

L. Hermosa Muñoz, I. Márquez, S. Cazzoli, J. Masegosa, and B. Agís-González

Instituto de Astrofísica de Andalucía - CSIC, Glorieta de la Astronomía s/n, 18008 Granada, Spain  
e-mail: lhermosa@iaa.es

Received M DD, YYYY; accepted M DD, YYYY

## ABSTRACT

*Context.* Outflows play a major role in the evolution of galaxies. However, we do not have yet a complete picture of their properties (extension, geometry, orientation and clumpiness). For low-luminosity Active Galactic Nuclei (AGNs), in particular, low-ionisation nuclear emission line regions (LINERs), the rate of outflows and their properties are largely unknown.

*Aims.* The main goal of this work is to create the largest, up-to-date atlas of ionised gas outflow candidates in a sample of 70 nearby LINERs. We aim to use narrow-band, imaging data to analyse the morphological properties of the ionised gas nuclear emission of these galaxies and to identify signatures of extended emission with distinctive outflow-like morphologies.

*Methods.* We obtained new imaging data from Alhambra Faint Object Spectrograph and Camera (ALFOSC)/Nordic Optical Telescope (NOT) for a total of 32 LINERs, and complemented it with Hubble Space Telescope archival data (HST) for 6 objects. We extracted the H $\alpha$  emission of the galaxies and used it to morphologically classify the circumnuclear emission. We combined our results with those from the literature for additional 32 targets. We additionally obtained soft X-ray data from Chandra archive to compare this emission with the ionised gas.

*Results.* The distribution of the ionised gas in these LINER indicates that  $\sim 32\%$  show bubble-like emission,  $\sim 28\%$  show a ‘Core-halo’, unresolved emission, and  $\sim 21\%$  of the sample have a disk-like distribution. Dust lanes prevent any detailed classification for  $\sim 11\%$  of the sample, that we call as ‘Dusty’. The soft X-ray emission is in most cases ( $\sim 60\%$ ) co-spatial with the ionised gas. If we account for the kinematical information which is available for a total of 60 galaxies, we end up with a total of 48% of the LINERs with detected outflows/inflows in the emission lines (50% considering only kinematical information based on Integral Field Spectroscopic data).

*Conclusions.* Our results suggest that the incidence of outflows in LINERs may vary from 41% up to 56%, based on both the H $\alpha$  morphology and the kinematical information from the literature. The ionised gas seems to be correlated with the soft X-ray emission, so that they may have a common origin. We discuss the use of H $\alpha$  imaging for the pre-selection of candidates likely hosting ionised gas outflows.

**Key words.** galaxies: active – galaxies: nuclei – galaxies: structure – galaxies: kinematics and dynamics – galaxies: statistics

## 1. Introduction

Outflows are believed to play an important role in the evolution of galaxies (e.g. Kormendy & Ho 2013; Cresci & Maiolino 2018; Veilleux et al. 2020). Those driven by Active Galactic Nuclei (AGNs) interact with the gas in the host galaxy generating both negative and positive feedback processes that affect the evolution of the host with notable effects, such as the gas-recycling or the suppression of the star formation (e.g. Fabian 2012; Cresci & Maiolino 2018). Outflows are characterised by their multi-wavelength phases (cold, warm and ionised gas), whose analysis is needed to fully understand their importance on the evolution of their host galaxies (e.g. Cazzoli et al. 2014; Cicone et al. 2014; Ramos Almeida & Ricci 2017; Morganti 2017; Veilleux et al. 2020; Fluetsch et al. 2021).

These galactic outflows are commonly seen in all AGN types (e.g. Veilleux et al. 2005; Morganti 2017; Veilleux et al. 2020), including a handful of Low-Ionisation Nuclear Emission-line Regions (LINERs) (Heckman 1980). Given that the presence of

outflows has been suggested to be ubiquitous within the AGN population (e.g. Veilleux et al. 2005; Concas et al. 2019), it is also expected to be the case for low-luminosity AGNs, as LINERs. Although that, this field is largely unexplored except for few works (Cazzoli et al. 2018; Hermosa Muñoz et al. 2020). This is probably a result of a bias towards the search of outflows in powerful AGNs, where these outflows are more easily identified, as the outflow rate scales with the AGN luminosity (Fluetsch et al. 2019). Nevertheless, much less is known for the largest population of AGNs in the Local Universe, which is dominated by LINERs (Ho et al. 1997). Mainly hosted in early-type galaxies (Ho 2008), their AGN nature is not yet clear for all the objects (Márquez et al. 2017), given the existence of other mechanisms, such as shocks (Heckman 1980; Dopita & Sutherland 1995; Molina et al. 2018), that could explain the observed spectra of these systems.

One of the best ways to identify the presence of outflows is using kinematical information via 2D spectroscopy (e.g. Davies et al. 2014; Harrison et al. 2016; Mingozzi et al. 2019; Davies et al. 2020; Cazzoli et al. 2020; Raimundo 2021, Cazzoli et al. in prep). These spectroscopic measurements allow us to obtain resolved information of the gaseous component of a galaxy at low (e.g. Raimundo 2021) and high redshift (e.g.

<sup>★</sup> Based on observations made with the Nordic Optical Telescope, operated by the Nordic Optical Telescope Scientific Association at the Observatorio del Roque de los Muchachos, La Palma, Spain, of the Instituto de Astrofísica de Canarias.

Harrison et al. 2016). In more luminous AGNs, the kinematical component of the emission lines associated to the outflow can dominate and be the more predominant feature of the spectra, above other rotational movements of the internal gas (Davies et al. 2020). However, in the absence of spectroscopic data, outflows may be detected, or at least hinted by using imaging techniques, even when the activity of the host galaxy is low (Masegosa et al. 2011). In the works by Pogge et al. (2000) and Masegosa et al. (2011) they studied the extended ionised  $H\alpha$  emission of several LINER-like galaxies. In the latter work, this emission was classified in different morphological types depending on the distribution of the ionised gas. One of the possible classification is outflow-like, referred to extended filamentary or bubble-like gas extending out of the galaxy nuclei. For some galaxies, this ionised gas emission with morphological signatures of outflowing gas, was later confirmed as an outflow by means of the use of kinematic data obtained from 2D spectroscopy (see e.g. NGC 4676A in Wild et al. 2014).

In this paper, our objectives are: (i) to create an atlas of the ionised gas morphology of a sample of nearby ( $z < 0.025$ ) LINERs that almost doubles that previously existing; (ii) search for morphological evidences of possible outflowing gas that could be associated to feedback processes, in order to determine how common outflows/inflows may be for the LINER AGN family; (iii) compare the  $H\alpha$  morphology to that seen in X-rays (when possible), to investigate possible correlations between both emissions, as seen in different AGN types in previous works (Bianchi et al. 2006; Masegosa et al. 2011; Bianchi et al. 2019); and (iv) look for kinematically-identified outflows in the literature within our targets, in order to test the goodness and eventual relation of the morphological signatures in the actual detection of outflows.

This paper is organised as follows: Section 2 describes the selection of the sample and the data gathering. In Section 3 we present the data reduction. In Section 4 we show the main results of the  $H\alpha$  and X-ray morphologies. We discuss the kinematical signatures of outflows identified in the literature for our targets, its relation with the gas morphology, as well as the implications of our work in Section 5. Finally, Section 6 summarises the main conclusions. Individual comments on each galaxy are in Appendix A; all the figures can be found in Appendix B.

## 2. Sample and data

The total number of objects analysed in this work is 70 LINERs (see Table 1), that were selected as explained below. The parent sample of our data set comes from González-Martín et al. (2009), where the X-rays properties of 82 LINERs were analysed, and is complemented with 11 LINERs from Cazzoli et al. (2018) and 2 from Pogge et al. (2000). We included in the sample one additional LINER (NGC 5957) not initially in either of the initial samples, but for which we have integral field spectroscopic data (Hermosa Muñoz et al. in prep). To select the targets, we applied the following criteria: (i) all galaxies should have distances not larger than 100 Mpc in order to ensure that the galaxies fitted in the field-of-view (FoV) allowing to detect parsec-scale structures; (ii) we do not consider systems on a high level of interaction. The first criterion excluded 14 galaxies and the second excluded 5 objects. This lead to 77 objects, from which 36 were already studied either in Masegosa et al. (2011) (hereafter M11) or in Pogge et al. (2000) (32 from the first, 4 from the second). Among the 32 targets in M11 we found NGC 4676A and B, that are on a high interacting level, so we further excluded

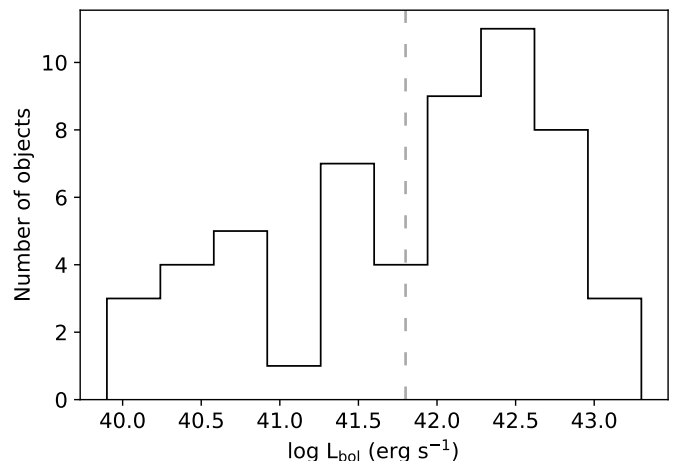


**Fig. 1.** Histogram of the bolometric luminosities (in log units) of the selected sample of LINERs. The luminosities were estimated from González-Martín et al. (2009) (see Table 1). The dashed grey line indicates the average value ( $10^{41.8}$  erg s<sup>-1</sup>).

them. We added NGC 3379 and NGC 4278 to the remaining 41 targets, as they were analysed in M11 based only in the  $H\beta$ , but not in the  $H\alpha$  emission. Thus, we end up with 43 LINERs; from them, we were able to gather data for 38 targets (see Table 2, Table 3 and Sect. 2.1).

To achieve the largest statistics of  $H\alpha$  images possible, our final sample encompass the 38 new targets with those from M11 and Pogge et al. (2000) with previous observations (32 targets, excluding NGC 3379, NGC 4278, NGC 4676A and B). Hence, summing up, the complete sample we analysed is 70 LINERs. We estimated the bolometric luminosity of the sources with the X-ray luminosity (2-10 keV) following González-Martín et al. (2009) (see Fig. 1). The typical bolometric luminosity of our sources is  $10^{41.8}$  erg s<sup>-1</sup> (see Table 1).

### 2.1. Data gathering

We searched for archival data in any available narrow filter from the HST for the 43 objects that corresponded to the  $H\alpha$  line at the redshift of the targets, finding 6 objects with at least one image available (see Table 2). The selected filters are indicated for each object in Table 2. We aimed to observe the remaining 37 objects with the Alhambra Faint Object Spectrograph and Camera (ALFOSC), at the Nordic Optical Telescope (NOT), during several observing campaigns (see Table 3).

The ALFOSC instrument is located at the NOT telescope (2.56 m), in ‘Roque de los Muchachos’ observatory, in La Palma, Spain. We used its camera in imaging mode, with a total FoV of  $6.4' \times 6.4'$  and a pixel scale of  $0.214'' \text{pix}^{-1}$ .

The data were gathered in a total of 14 nights (PIs: S. Cazzoli and L. Hermosa Muñoz; see Table 3). We obtained 3 individual exposures for both narrow and broad band filters per galaxy, with typical exposure times of 1200 s and 300 s, respectively. For some objects, the broad filter images were observed with smaller exposure time to avoid saturation of the galaxy centre. The total time on source per galaxy was 1.25 hours. The average seeing and airmass were  $0.92''$  and 1.24, respectively (the corresponding information for the different nights is listed in Table 3).

We used the narrow filters from NOT that allowed us to observe the ionised gas of the LINERs at their given redshift, that corresponded to the  $H\alpha$  line. These are (as indicated in

the NOT web page<sup>1</sup>): #49 (661.5 - FWHM 50Å), #50 (665.5 - FWHM 55Å), #68 (664.4 - FWHM 40Å), #77 (662.4 - FWHM 39Å), #78 ([N II] $\lambda$ 658.4 - FWHM 36Å) and #123 ([S II]  $\lambda$ 672.5 - FWHM 50Å). As for the broad filter, we used the standard R band filter from the Sloan Digital Sky Survey (as indicated in the NOT web page: r'\_SDSS 625\_140 - FWHM 1400Å). The selected narrow filters are wide enough to also include one of the [N II] $\lambda$ 6548,6584Å emission lines. However, we have chosen the filters such that the only other emission line that could also fit within the filter is the [N II] $\lambda$ 6548Å line, which is weaker than the [N II] $\lambda$ 6584Å line (relation 1:3, see Osterbrock & Ferland 2006). Contamination of the H $\alpha$  line due star-formation processes could exist. However, we do not expect this to be important, as all our sources are early-type galaxies (see morphological types in Table 1), where the star formation is expected to be less important than in later host types.

The presence of several ghosts contaminated the images of NGC 0474 and NGC 0524, observed with the NOT filter #77. This prevented a reliable analysis and therefore, these two galaxies were further excluded from the sample. NGC 5957 was observed while high clouds appeared during at least one individual exposure, dimming the object flux. Finally, due to bad weather conditions and time constraints to finish the last observing run, 3 objects (NGC 0833, NGC 0835 & NGC 2655) were not observed. Thus, the campaign is completed up to a ~90% of the sample (37 objects).

## 2.2. X-ray data

We searched for X-ray data in the Chandra Data Archive for all the new galaxies in the sample (38 objects) for which we obtained optical data, to compare their soft emission (0.3 - 2 KeV) with the ionised gas. We retrieved X-ray images taken with the Advanced CCD Imaging Spectrometer (ACIS) for a total of 28 objects. We estimated the  $3\sigma$  contours of the emission and superimposed them to the H $\alpha$  images.

For the data coming from M11, there is a similar analysis with both hard and soft X-ray Chandra images. They gathered data for a total of 26 objects, whose results we discuss in Sect. 5.2. The images from their objects can be found in their Fig. 6.

## 2.3. Kinematical information

By searching in the literature, we retrieved kinematical information either for all the LINERs from Integral Field Spectroscopy (IFS) (30 galaxies) or long-slit spectroscopic data (30 galaxies). When a target was analysed with IFS data, we prioritised those 3D results over those coming from long-slit spectroscopy. The previous works analysing the different targets (see Sect. 5.1 and Appendix A for more details on the individual sources) discuss the possible presence of outflows/inflows or non-rotational motions in the galaxies for 28 objects. We compare the morphologically-identified outflows with those kinematically-identified (or undetected) in Sect. 5.1.

<sup>1</sup> <http://www.not.iac.es/instruments/filters/filters.php>

**Table 1.** General properties for all the 70 LINERs in this paper. The line separates the new observed targets from those selected from Masegosa et al. (2011) and Pogge et al. (2000). (3) RA and (4) DEC: coordinates; (5) Morphology, (6)  $z$  and (7) scale distance: from the Local Group from NED; (8)  $i$ : inclination angle from Ho et al. (1997); (9)  $V$  magnitude from HyperLeda; and (10) bolometric luminosity estimated from (González-Martín et al. 2009). <sup>(\*)</sup> indicates galaxies observed with high clouds; <sup>†</sup> indicates targets already analysed in Masegosa et al. (2011).

#	ID	Other name	RA (hh mm ss) (3)	DEC (dd mm ss) (4)	Morphology (5)	$z$ (6)	Scale (pc arcsec <sup>-1</sup> ) (7)	$i$ (deg) (8)	$V$ mag (9)	$L_{\text{bol}}$ ( $10^X$ ) (erg s <sup>-1</sup> ) (10)
1	NGC 0266	UGC 508	00 49 47.80	+32 16 39.79	SB(rs)ab	0.0155	351	12	11.8	–
2	NGC 0410	UGC 735	01 10 58.90	+33 09 06.81	E+	0.0177	395	–	11.5	42.25
3	NGC 0841	IRAS 02082+3715	02 11 17.36	+37 29 49.80	(R')SAB(s)ab	0.0151	339	57	13.1	–
4	NGC 2685	IRAS 08517+5855	08 55 34.71	+58 44 03.83	(R)SB0+pec	0.0030	70	60	11.4	42.35
5	NGC 3185	HCG 44c	10 17 38.56	+21 41 17.70	(R)SB(r)a	0.0041	79	48	12.2	42.68
6	NGC 3379 <sup>†</sup>	M 105	10 47 49.59	+12 34 53.85	E1	0.0030	55	–	9.3	41.44
7	NGC 3414	IRAS 10485+2814	10 51 16.21	+27 58 30.36	S0 pec	0.0049	100	44	11.1	41.39
8	NGC 3507	UGC 6123	11 03 25.36	+18 08 07.62	SB(s)b	0.0033	62	32	–	<40.51
9	NGC 3608	UGC 6299	11 16 58.95	+18 08 55.26	E2	0.0041	80	–	10.6	41.51
10	NGC 3628	IRAS 11176+1351	11 20 16.97	+13 35 22.86	Sb	0.0028	51	–	9.5	41.47
11	NGC 3642	IRAS 11194+5920	11 22 17.89	+59 04 28.25	SA(r)bc	0.0053	121	34	12.2	–
12	NGC 3884	UGC 6746	11 46 12.18	+20 23 29.93	SA(r)0/a	0.0233	496	51	12.6	–
13	NGC 3898	IRAS 11465+5621	11 49 15.37	+56 05 03.69	SA(s)ab	0.0039	91	55	10.7	<42.08
14	NGC 3945	IRAS 11506+6056	11 53 13.73	+60 40 32.00	SB(rs)0	0.0043	100	50	10.8	40.66
15	NGC 4125	IRAS 12055+6527	12 08 06.02	+65 10 26.90	E6 pec	0.0060	107	–	9.7	<42.04
16	NGC 4143	UGC 7142	12 09 36.06	+42 32 03.00	SAB(s)0	0.0032	70	52	12.1	–
17	NGC 4203	IRAS 12125+3328	12 15 05.05	+33 11 50.38	SAB0-	0.0036	77	21	11.6	–
18	NGC 4261	3C 270	12 19 23.22	+05 49 30.78	E2-3	0.0074	148	–	11.1	42.60
19	NGC 4278 <sup>†</sup>	IRAS 12175+2933	12 20 06.82	+29 16 50.72	E1-2	0.0021	42	–	10.2	42.53
20	NGC 4321	M 100	12 22 54.83	+15 49 18.54	SAB(s)bc	0.0052	106	32	9.5	42.03
21	NGC 4450	IRAS 12259+1721	12 28 29.63	+17 05 05.81	SA(s)ab	0.0065	134	43	10.9	–
22	NGC 4457	IRAS 12264+0350	12 28 59.01	+03 34 14.09	(R)SAB(s)0/a	0.0029	53	32	10.6	42.12
23	NGC 4459	IRAS 12264+1415	12 29 00.01	+13 58 42.14	SA(r)0+	0.0040	78	41	10.3	39.90
24	NGC 4494	IRAS 12288+2603	12 31 24.10	+25 46 30.91	E1-2	0.0045	93	–	9.8	40.31
25	NGC 4589	IRAS 12353+7428	12 37 24.99	+74 11 30.92	E2	0.0066	155	–	10.7	42.23
26	NGC 4596	IRAS 12373+1027	12 39 55.95	+10 10 34.10	SB(r)0+	0.0063	128	43	10.5	40.00
27	NGC 4698	IRAS 12458+0845	12 48 22.91	+08 29 14.58	SA(s)ab	0.0034	64	53	10.7	42.05
28	NGC 4750	IRAS 12483+7308	12 50 07.27	+72 52 28.72	(R)SA(rs)ab	0.0054	129	24	12.1	–
29	NGC 4772	UGC 8021	12 53 29.16	+02 10 06.16	SA(s)a	0.0035	65	62	11.3	–
30	NGC 5077	UGCA 347	13 19 31.67	–12 39 25.07	E3-4	0.0094	188	–	11.7	–
31	NGC 5363	IRAS 13356+0529	13 56 07.21	+05 15 17.18	I0?	0.0038	76	51	10.2	43.09
32	NGC 5746	IRAS 14424+0209	14 44 55.92	+01 57 18.01	SAB(rs)b	0.0058	120	–	10.6	41.75
33	NGC 5813	UGC 9655	15 01 11.23	+01 42 07.13	E1-2	0.0065	138	–	10.5	42.08
34	NGC 5838	IRAS 15029+0217	15 05 26.26	+02 05 57.59	SA0-	0.0045	94	72	10.8	42.51
35	NGC 5957 <sup>(*)</sup>	IRAS 15330+1212	15 35 23.21	+12 02 51.36	(R')SAB(r)b	0.0061	134	–	12.3	–
36	NGC 6482	UGC 11009	17 51 48.81	+23 04 18.99	E	0.0131	296	–	11.3	42.64
37	NGC 7331	IRAS 22347+3409	22 37 04.01	+34 24 55.87	SA(s)b	0.0038	80	72	9.4	41.76
38	NGC 7743	IRAS 23417+0939	23 44 21.14	+09 56 02.69	(R)SB(s)0+	0.0057	138	32	12.4	<42.86
39	IC 1459	IRAS 22544-3643	22 57 10.61	-36 27 44.00	E3-4	0.0060	131	–	10.5	–
40	NGC 0315	UGC 00597	00 57 48.88	+30 21 08.81	E+	0.0165	370	52	11.6	43.30
41	NGC 0404	IRAS 01066+3527	01 09 27.02	+35 43 05.27	SA0(s)	-0.0002	–	–	10.6	–
42	NGC 1052	IRAS 02386-0828	02 41 04.80	-08 15 20.75	E4	0.005	108	–	11.0	42.77
43	NGC 2639	IRAS 08400+5023	08 43 38.08	+50 12 20.00	(R)SA(r)a	0.0111	242	54	11.8	<41.59
44	NGC 2681	IRAS 08499+5130	08 53 32.73	+51 18 49.30	(R)SAB(rs)0/a	0.0023	24	–	10.9	42.58
45	NGC 2787	IRAS 09148+6924	09 19 18.56	+69 12 12.00	SB0+(r)	0.0023	60	51	11.3	<40.34
46	NGC 2841	IRAS 09185+5111	09 22 02.63	+50 58 35.47	SA(r)b	0.0021	49	66	10.2	40.75
47	NGC 3226	ARP 094	10 23 27.01	+19 53 54.68	E2 pec	0.0044	86	–	12.9	42.33
48	NGC 3245	IRAS 10244+2845	10 27 18.39	+28 30 26.56	SA0 <sup>0</sup> (r)	0.0044	90	58	10.8	42.29
49	NGC 3607	UGC 06297	11 16 54.66	+18 03 06.50	SA0 <sup>0</sup> (s)	0.0031	58	62	10.0	42.07
50	NGC 3623	M 65	11 18 55.96	+13 05 32.00	SAB(rs)a	0.0027	48	77	9.3	<40.91
51	NGC 3627	M 66	11 20 15.03	+12 59 29.58	SAB(s)b	0.0024	42	65	10.3	42.72
52	NGC 3718	ARP 214	11 32 34.85	+53 04 04.52	SB(s)a pec	0.0033	76	62	10.7	–
53	NGC 3998	UGC 06946	11 57 56.13	+55 27 12.92	SA0 <sup>0</sup> (r)	0.0035	82	34	11.3	42.85
54	NGC 4036	IRAS 11588+6210	12 01 26.75	+61 53 44.81	S0 <sup>-</sup>	0.0046	108	69	10.8	42.43
55	NGC 4111	UGC 07103	12 07 03.13	+43 03 56.59	SA0 <sup>0</sup> (r)	0.0026	59	85	10.8	<41.89
56	NGC 4192	M 98	12 13 48.29	+14 54 01.20	SAB(s)ab	-0.0005	–	78	10.8	–
57	NGC 4314	IRAS 12200+3010	12 22 31.82	+29 53 45.19	SB(rs)a	0.0032	67	27	10.6	<40.63
58	NGC 4374	M 84	12 25 03.74	+12 53 13.14	E1	0.0034	65	–	9.8	42.84
59	NGC 4438	IRAS 12252+1317	12 27 45.59	+13 00 31.78	SA(s)0/a pec	0.0002	–	71	10.9	<42.36
60	NGC 4486	M 87	12 30 49.42	+12 23 28.04	E	0.0043	84	–	9.0	42.35
61	NGC 4552	M 89	12 35 39.81	+12 33 22.83	E0-1	0.0011	17	–	10.1	40.78



**Table 1.** Continue.

#	ID	Other name	RA (hh mm ss)	DEC (dd mm ss)	Morphology	z	Scale (pc arcsec <sup>-1</sup> )	<i>i</i> (deg)	V mag	L <sub>bol</sub> (10 <sup>X</sup> ) (erg s <sup>-1</sup> )
	(1)	(2)	(3)	(4)	(5)	(6)	(7)	(8)	(9)	(10)
62	NGC 4579	M 58	12 37 43.52	+11 49 05.50	SAB(rs)b	0.0051	101	38	10.3	42.70
63	NGC 4594	M 104	12 39 59.43	-11 37 22.99	SA(s)a	0.0034	59	68	8.6	41.50
64	NGC 4636	UGC 07878	12 42 49.83	+02 41 15.99	E0-1	0.0031	57	–	9.9	<40.56
65	NGC 4696	ABELL 3526:BCG	12 48 49.27	-41 18 40.04	cD1 pec	0.0099	193	–	10.3	41.51
66	NGC 4736	M 94	12 50 53.06	+41 07 13.65	(R)SA(r)ab	0.0010	25	36	9.5	40.13
67	NGC 5005	IRAS 13086+3719	13 10 56.23	+37 03 33.14	SAB(rs)bc	0.0032	70	63	10.7	<43.16
68	NGC 5055	M 63	13 15 49.33	+42 01 45.40	SA(rs)bc	0.0017	40	56	8.6	41.09
69	NGC 5846	UGC 09706	15 06 29.28	+01 36 20.25	E0-1	0.0057	121	–	10.2	<42.34
70	NGC 5866	M 102	15 06 29.49	+55 45 47.57	SA0+	0.00001	13	68	11.3	41.60

### 3. Data reduction process

The data gathered from the HST archive were already fully reduced and the narrow-band images of the galaxies were already combined in those cases where there was more than one available. However, given that the HST observations are from the archive, some of the selected narrow filter (NF) images were not observed the same night as the broad filter (BF) images (see Table 2). We tried to select, when possible, the BF with the closest wavelength range to the NF range. Thus, the only procedure applied to HST data was the realignment of the NF and BF images when they were obtained in different observing campaigns (see Table 2). Specifically, we used the position angles on the header of the different frames to set the images to a common North-East axis reference. Then the outermost, elliptical isophotes were fitted to ellipses, providing us with the centres and position angles that were used to apply the corresponding shift and rotation for alignment. Finally, we trimmed the images to where both had information.

The data from ALFOSC/NOT were reduced following standard procedures (bias and flat-fielding) with both IRAF<sup>2</sup> and PYTHON routines. We performed a dedicated background subtraction to the ALFOSC/NOT images required for a reliable sky determination. An example of the procedure is shown in Fig. 2. We used PHOTUTILS routines under a PYTHON environment to mask external stars, galaxies and artefacts from the filter, and estimate a 2D background. We created masks for objects detected at least at  $3\sigma$  over the background in the BF images (as usually the flux is more extended in this filter) and applied them to the NF ones. The background in the masked pixels could not be estimated, so we used the median value of the background in the rest of the image. Then, we made a smoothing of the background image (100 $\times$ 100 pixels), so that no structures were included due to the masks, and we subtracted the final smoothed background image per each galaxy and filter.

In order to obtain exclusively the emission of the galaxies in the H $\alpha$  line, we subtracted the continuum of the narrow-band images using broad-band images of the same targets. For ALFOSC/NOT, those BF images were observed the same night as the NF ones. The procedure follows that from M11. The NF images include not only the H $\alpha$  emission but also the underlying continuum. The line emission is usually less extended than the continuum, which is translated into the fact that, at large scales in the galaxy, both NF and BF images should return comparable emissions. Thus, we scaled the BF image to the NF image and then subtract them to obtain the H $\alpha$  image.

The peculiar morphologies of the galactic continuum in the studied galaxies are highlighted by the use of sharp-divided images (e.g. Márquez & Moles 1996; Márquez et al. 1999, 2003). Briefly, this technique consists on dividing the BF image by its smoothed version, which is the original image convolved with a median filter of a 20-pixel box. Although simple, this method is very useful specially for detecting asymmetries on the image, such as bars, rings, spiral arms or dust regions. The sharp-divided images of the galaxies are shown in the right panels of Appendix B.

<sup>2</sup> IRAF is the Image Reduction and Analysis Facility distributed by the National Optical Astronomy Observatories (NOAO) for the reduction and analysis of astronomical data. <http://iraf.noao.edu/>

The Chandra X-ray images were reduced following the Chandra threads aimed for the ACIS instrument, using the dedicated software CIAO v4.13 and the calibration package CALDB 4.9.5. After downloading the data, we applied the most recent calibrations running the script ‘chandra\_repro’ and restricted to the energy range between 0.3-2 KeV. We extracted background light curves from the event files using the CIAO tool DMEXTRACT in order to eliminate high background events. Based on those background light curves, we generated Good Time Intervals for our images excluding time intervals deviated  $1\sigma$  from the mean rate of counts in the background using the CIAO tool DEFLARE.

### 4. Results

We have classified the circumnuclear H $\alpha$  morphologies of the galaxies according to 4 different categories: ‘Core-halo’, ‘Disky’, ‘Bubble’ and ‘Dusty’. An example of each morphological type is shown in Fig. 3. The properties of the ionised emission included in these categories are fully explained in M11. The basic definitions are: (i) ‘Core-halo’: unresolved nuclear emission in the galaxy centre; (ii) ‘Disky’: ionised emission along spiral arms, star forming rings or diffuse emission in the disc; (iii) ‘Bubble’: equivalent to the ‘Outflow’ morphology in M11, refers to biconical, filamentary or bubble-like structures emerging from the nucleus; and (iv) ‘Dusty’: mostly edge-on galaxies with dust lanes obscuring the nuclear emission. We classified all the targets using visual inspection of the H $\alpha$  images, considering all the emission detected above  $3\sigma$  from the background. Our classification is given in Table 4. We assigned a morphological class when 3 or more authors agreed on the classification. This happened for 87% of the targets from the new data. The remaining 13% (5 out of 38) had ambiguous morphologies that could be included in various classes. To enable a more clear discussion, we defined for them the additional category ‘Unclear’. In this Section we account only for the new observed data, as the results for the other targets are presented in M11 and Pogge et al. (2000). More details on the individual galaxies can be found in Appendix A; all H $\alpha$  and sharp-divided images are in Appendix B, and the soft X-ray images (in contours) are in Fig. 5.

#### 4.1. Ionised-gas morphological classification

We have identified a total of 12 LINERs that show ‘Core-halo’ emission. Among them, NGC 4261, NGC 4589 and NGC 6482 (see Figs. B.5, B.7 and B.9, respectively) show extended emission probably elongated along their galaxy disks; NGC 3884, NGC 4278, NGC 4772 and NGC 5957 (see Figs. B.3, B.5, B.8 and B.9, respectively) have an unresolved, not elongated nuclear emission; in the remaining galaxies, NGC 0410, NGC 4450, NGC 4494, NGC 4698 and NGC 7743 (see Figs. B.1, B.6, B.7 and B.10), the H $\alpha$  emission is extended and detected at  $3\sigma$  level at distances larger than  $>10''$  from their nuclei.

The ‘Disky’ morphology is found in 9 galaxies. For NGC 0841, NGC 3642, NGC 4321 and NGC 4457 (see Figs. B.1, B.3, B.5 and B.6) the emission is found along a star-formation ring or arm, where several clumps are easily identified. In 3 galaxies, namely NGC 3185, NGC 3507 and NGC 5077 (see Figs. B.2 and B.8), the emission shows a twisted and elongated shape that may be ascribed to a bar or to large-scale spiral arms or discs. Finally, for 2 galaxies, NGC 3608 and NGC 3898 (see Figs. B.3 and B.4, respectively), the emission is extended along the disc, with no clumps or evidence of star formation.

**Table 2.** Observing log of HST data. Columns indicate: (1) galaxy name; (2) observing instrument; (3) file name of the image as indicated in the archive; (4) proposal ID of the observations; (5) Principal Investigator of the proposal; (6) date of the observation; (7) exposure time; (8) filter used, also from the HST archive.

ID	Instrument	Filename (.fits)	Proposal ID	P.I.	Obs. date (yy-mm-dd)	Exp. time (s)	Filter
(1)	(2)	(3)	(4)	(5)	(6)	(7)	(8)
NGC 3642	ACS/WFC	<i>hst_9788_41_acs_wfc_f658n</i>	9788	L. Ho	2003-12-16	700	F658N
	ACS/WFC	<i>hst_9788_41_acs_wfc_f814w</i>	9788	L. Ho	2003-12-16	120	F814W
NGC 4125	WFPC2	<i>hst_11966_15_wfpc2_f658n_wf</i>	11966	M. Regan	2009-01-30	2100	F658N
	WFPC2	<i>hst_06587_23_wfpc2_f555w_wf</i>	6587	D.Richstone	1997-03-15	1400	F555W
NGC 4203	ACS/WFC	<i>hst_9788_72_acs_wfc_f658n</i>	9788	L. Ho	2003-07-18	700	F658N
	ACS/WFC	<i>hst_9788_72_acs_wfc_f814w</i>	9788	L. Ho	2003-07-18	120	F814W
NGC 4450	WFPC2	<i>hst_11966_18_wfpc2_f658n_wf</i>	11966	M. Regan	2009-01-31	1800	F658N
	WFPC2	<i>hst_05375_04_wfpc2_f555w_wf</i>	5375	V.Rubin	1994-05-09	520	F555W
NGC 4750	ACS/WFC	<i>hst_9788_b4_acs_wfc_f658n</i>	9788	L. Ho	2004-05-20	700	F658N
	ACS/WFC	<i>hst_9788_b4_acs_wfc_f814w</i>	9788	L. Ho	2004-05-20	120	F814W
NGC 7331	WFC3	<i>hst_14202_01_wfc3_uvis_f657n</i>	14202	D.Milislavljevic	2015-08-22	2400	F657N
	WFC3	<i>hst_14202_01_wfc3_uvis_f814w</i>	14202	D.Milislavljevic	2015-08-22	1350	F814W

**Table 3.** Observing log of ALFOSC/NOT data. Columns indicate: (1) observing campaign; (2) date of the observation; (3) number of galaxies observed ; (4) exposure time for the narrow (broad) filter; (5) range of the airmass; (6) seeing range during the observations.

Observing campaign	Observing date (yy-mm-dd)	Observed galaxies (3)	Exposure time NF-BF (s)	Airmass (5)	Seeing (6)
(1)	(2)	(3)	(4)	(5)	(6)
GT-Jan2019	2019-01-03	NGC 0841/NGC 2685/NGC 3185 NGC 3884/NGC 4278	1200 (300)	1.01-1.42	0.7''-1.5''
	2019-01-04	NGC 0266/NGC 0410/NGC 3414/NGC 4143	1200 (300)	1.03-1.7	0.6''-1.8''
	2019-01-05	NGC 3507/NGC 4698/NGC 4772	1200 (300)	1.06-1.5	0.7''-1.3''
GT-May2019	2019-05-31	NGC 3628	1200 (300)	1.10-1.30	0.8''-0.9''
	2019-06-01	NGC 5363	1200 (100)	1.09-1.16	0.9''-1.6''
GT-Jan2020	2020-01-25	NGC 3379	1200 (300)	1.04-1.19	0.7''-0.9''
	2020-01-26	NGC 3608/NGC 3945/NGC 4596	1200 (300)	1.07-1.29	0.6''-0.9''
GT-Jun2021	2021-06-11	NGC 4494	1200 (100)	1.18-1.30	0.8''-0.9''
	2021-06-12	NGC 6482	1200 (300)	1.04-1.10	0.8''-1.0''
OT-Mar2020	2020-03-29	NGC 3898/NGC 4321/NGC 4457/NGC 4459	1200 (300)	1.03-1.21	0.6''-1.1''
		NGC 5746/NGC 5813/NGC 5957			
OT-Jun2020	2020-06-08	NGC 5077	1200 (300)	1.33-1.43	0.7''-0.8''
	2020-06-09	NGC 4589	1200 (300)	1.54-1.70	0.7''-1.0''
Other	2020-11-09	NGC 7743	1200 (100)	1.12-1.39	0.7''-0.8''
	2021-02-15	NGC 4261 & NGC 5838	1200 (100)	1.10-1.42	0.8''-1.1''

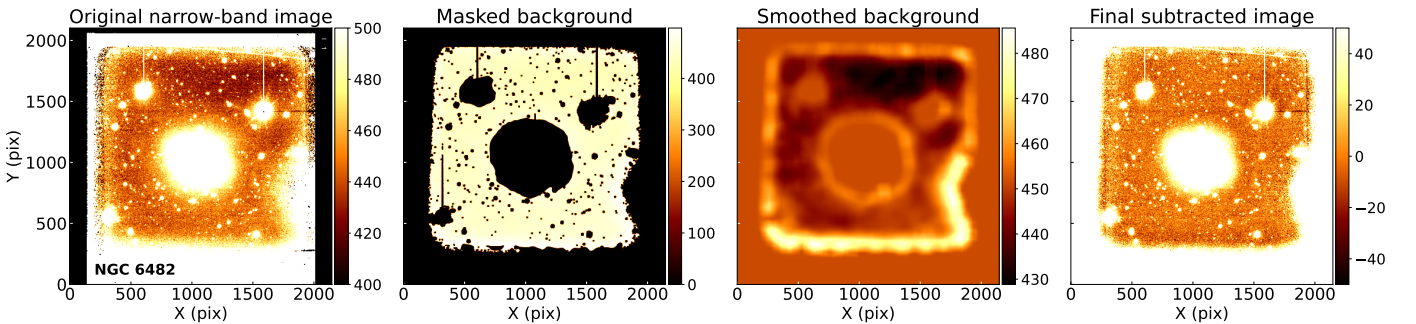


**Fig. 2.** Example of the background subtraction process for NGC 6482. *Left:* Original narrow-band image of the galaxy. *Middle-left:* Mask applied to the original image over imposed to the estimated background. *Middle-right:* Final smoothed background. *Right:* Final narrow-band image with the corresponding background subtracted. The scale on the left and right panels is around the background level to appreciate the differences before and after the subtraction. See Sect. 3 for more details.

There are only 3 objects classified as ‘Dusty’, as they show clear dust lanes that prevent from analysing their nuclear emission (NGC 3628, NGC 4125 and NGC 5746). However, note that this classification is based on the innermost regions ( $\sim 20''$ ) of the galaxies. NGC 3628 (Fig. B.3) is known to have extended

emission further out from the nuclei, a large scale  $H\alpha$  emission clearly visible in the southern parts of the galaxy (Fabbiano et al. 1990). In our image, this plume is barely detected at  $1\sigma$  level (see Fig. 4), whose analysis is out of the aim of this paper. NGC 4125 (Fig. B.4) has some extended emission, but clearly

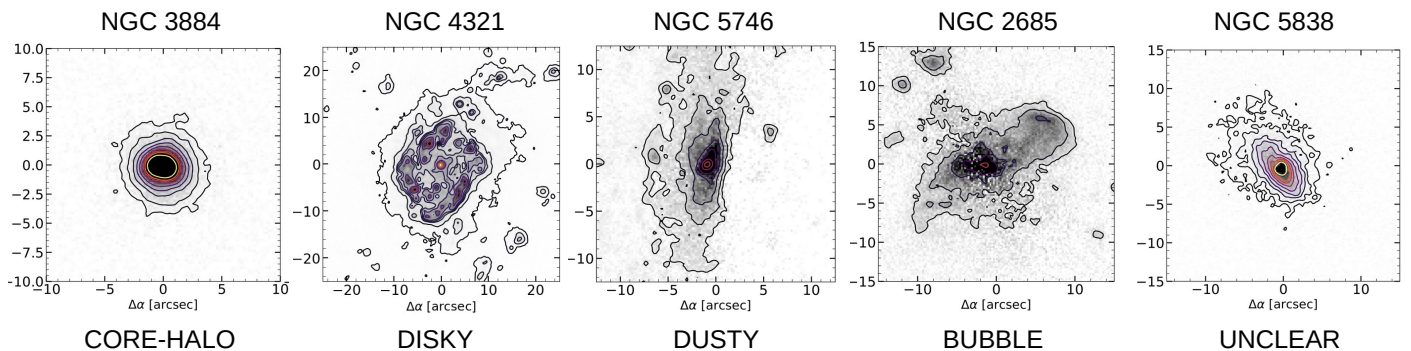


**Fig. 3.** Examples of the five proposed morphological classifications of the nuclear  $H\alpha$  emission (see Sect. 4). The complete images are in Appendix B.

around dust lanes, thus we were conservative in its classification. For NGC 5746 (Fig. B.8), the emission is barely visible through some regions of the galactic disc, thus not reliable for a proper morphological classification.

We have identified 9 LINERs that may have an outflowing emission with complex ionised gas morphologies. NGC 0266, NGC 3414, NGC 4596 and NGC 4750 (see Figs. B.1, B.2 and B.7) show a faint extended emission parting asymmetrically from the photometric centre of the galaxies. NGC 3945 image unveils a filamentary structure (Fig. B.4). For NGC 2685, NGC 3379 and NGC 5813 (see Figs B.1, B.2 and B.9), the  $H\alpha$  emission has a biconical or bubble-like shape oriented almost perpendicular to the major axis of the galaxies (inclination of NGC 2685 is  $60^\circ$ , not measured for the other two; see Table 1). NGC 4459 (see Fig. B.6) can also be included in this latter group, as the nuclear emission in the inner  $3'' \times 3''$  resembles the base of a outflowing bubble. All the objects would benefit of detailed spectroscopic information with spatial resolution to determine the extent and origin of their emission.

Finally, there are five galaxies (NGC 4143, NGC 4203, NGC 5363, NGC 5838 and NGC 7331) with ‘Unclear’ morphologies. NGC 4143, NGC 4203 and NGC 5838 are double classified in this work as ‘Bubble’ and ‘Disky’ (see Figs. B.4, B.5 and B.9). In these cases, the emission seems to be extended along the galaxy disc, but with a non-symmetrical distribution. These asymmetry may be produced due to outflows instead of being associated to the disc, which lead to the unclear classification. For the case of NGC 5363 (Fig. B.8), a nuclear dust lane of  $\sim 1$  kpc is obscuring the nucleus, although at larger scales ( $\geq 20''$ ) there is a extended, filamentary emission of ionised gas (see Fig. 4). The morphological differences at both scales lead to a double classification as ‘Dusty’, and ‘Bubble’. NGC 7331 (Fig. B.10) is classified as both ‘Dusty’ and ‘Bubble’, as we detect some extended emission out of the nucleus, but we cannot ensure this  $H\alpha$  profile to be symmetrical, as a thick dust lane is visible within the galaxy disc.

There are two galaxies, NGC 3379 and NGC 4278 (Figs. B.2 and B.5), that were observed in our sample despite they were also analysed in M11. The only available data in the HST archival were in the narrow filter corresponding to the [O III] line emission (filter F547M). In our work, we have obtained data for these galaxies in the  $H\alpha$  wavelength range, to have an uniform comparison of all the nuclear emissions in the galaxies from the sample. For M11, NGC 3379 (NGC 4278) was classified as having a ‘Disky’ (‘Core-halo’) emission. We agree on the classification of NGC 4278 but, on the contrary, we classified

NGC 3379 as having an ‘Bubble’, as the inner  $H\alpha$  morphology shows an elongated shape that cannot be ascribed to either of the other possible classifications. This elongated emission is coincident with a dust lane crossing the nuclear region, visible in  $H\beta$  (Masegosa et al. 2011). It could also be an effect produced by a bar (see individual comments on Appendix A), as the sharp-divided image (see Fig. B.2) show an ‘X’-like shape which is usually ascribed to barred systems (Laurikainen & Salo 2017).

#### 4.2. Soft X-ray images properties

Some previous works have studied the correlation between the soft X-ray and ionised gas emissions for different AGN types (Bianchi et al. 2006, ; M11), such that both emissions are believed to raise from the photoionisation of the gas around the AGN (Bianchi et al. 2006, 2019). These results are discussed in Sect. 5.2. For the new data, we searched for X-ray data with resolution comparable to that of the ALFOSC/NOT 38  $H\alpha$  images. The soft X-ray contours are shown in Fig. 5. The emission for 11 galaxies is mainly point-like around the nucleus, which would be equivalent to a ‘Core-halo’ classification (see Sect. 4). We find 12 objects with an extended emission and 5 with clumpy emission. Despite the different morphologies, the soft X-ray emission is co-spatial with the ionised gas for 12 galaxies (see Table 6).

If we separate those galaxies in which both emissions are coincident, at least, in the direction of the emission, we end up with 12 LINERs (NGC 0266, NGC 0410, NGC 3414, NGC 3884, NGC 3945, NGC 4261, NGC 4450, NGC 4596, NGC 4750, NGC 4772, NGC 5813, NGC 5838). One example is NGC 5813, for which the  $H\alpha$  image, specially at large scales, shows an extended filamentary structure (see Fig. 4), with a bubble extending up to  $10''$  in the north-west direction with respect to the centre. The X-ray emission is rather complex, with the same bubble almost co-spatial with the  $H\alpha$  emission (see Fig. 5).

The most notable difference in the remaining objects lies in the extension of the emission, being in some cases much more extended in the X-rays (e.g. NGC 4278, see Fig. B.5), and in other cases in  $H\alpha$  (e.g. NGC 4698, see Fig. B.7).

#### 4.3. Global picture of ionised gas morphologies in LINERs

For the new imaging data obtained with NOT and HST, as drawn by the detected  $H\alpha$  emission at  $3\sigma$  level, the nuclear ionised gas in these LINERs is extended ( $\geq 5''$ ) in the majority of the cases (32 objects;  $\sim 84\%$ ). This emission is not exclusively along



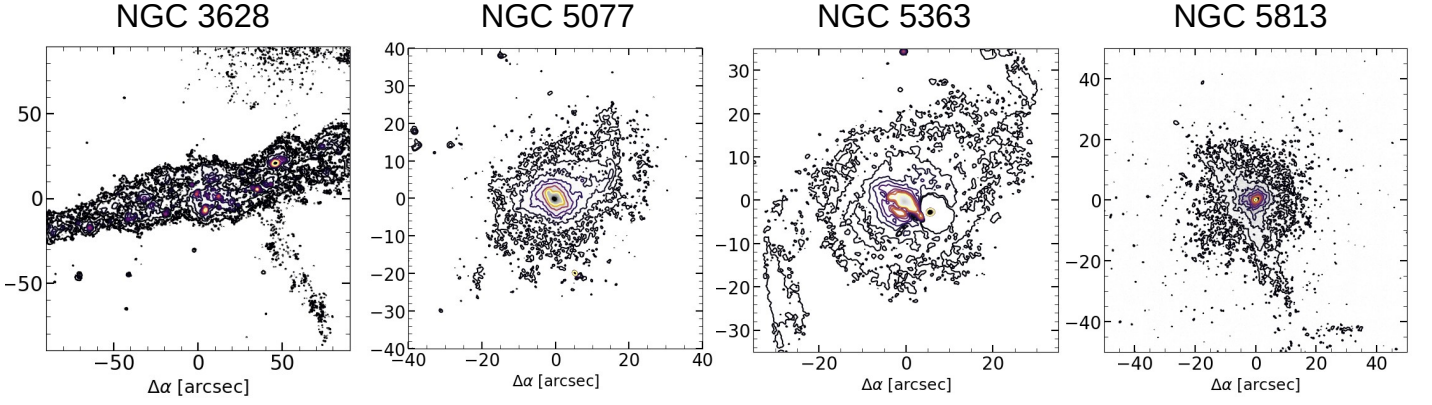


**Fig. 4.** Large-scale  $H\alpha$  images of NGC 3628, NGC 5077, NGC 5363 and NGC 5813. The largest contours indicate the  $1\sigma$  level over the background signal, except for NGC 5363, that represents  $3\sigma$ . The corresponding image on smaller scale ( $\sim 10'' \times 10''$ ) with the  $3\sigma$ -detection are shown in Appendix B.

spiral arms or nuclear discs but also due to possible outflows (for example, as filamentary structures), or perhaps other events at large scales (i.e.  $>1'$ ; see Fig. 4), as mergers (e.g. NGC 4125, see Appendix A and Fig. B.4).

Within our new data, as already mentioned in Sect. 4.1, we have 9 objects of outflow-like morphologies in the  $H\alpha$  nuclear emission, which corresponds to  $\sim 25\%$  of the sample. The same percentage also applies for disk-like emission (9 LINERs), whereas the majority are classified as ‘Core-halo’ (12 LINERs;  $\sim 32\%$ ). However, if we consider all the measurements and classifications in previous similar studies, larger statistics can be made. More specifically, in M11 they provided the final morphological classification for 30 LINERs, accounting for the data in Pogge et al. (2000) (see Sect. 2).

In this work, we have added a total of 38 new LINERs, considering both NOT and HST data sets. Summing up, we have  $H\alpha$  morphological information for a total of 70 LINERs, such that 32% of them are classified as having outflow-like emission, 29% show ‘Core-halo’ morphology, 21% are classified as ‘Disky’, 11% as ‘Dusty’ and 7% with an ‘Unclear’ morphology. These results indicate that 1 out of every 3 LINERs in the local Universe may have an outflow.

## 5. Discussion

The combined results of the new 38 objects from this work and 32 from previous works (Pogge et al. 2000; Masegosa et al. 2011) constitute the largest sample up to date of ionised gas morphological analysis of LINERs. The morphological features of the 70 galaxies indicate that a high percentage (32%) of LINERs do have outflow-like ionised gas emission. However, we notice that a dedicated spectroscopic follow-up using IFS is needed to firmly confirm what the morphological signatures suggest and capture the full extension of the putative outflow. This specially applies to the targets with long-slit spectroscopic observations, where the outflow will not be detected if the slit is not properly oriented.

We note that, although we classify all the images under the same criteria (see Sect. 4), both HST and ALFOSC/NOT data have different spatial resolutions. This implies a loss of detail on the possible substructures present on the images, but it should not produce any relevant change on the classification of the ionised gas morphology, as the categories defined rely on features

**Table 4.** Morphological classification of the  $H\alpha$  nuclear emission as in M11. The † indicates the galaxies classified in M11 and Pogge et al. (2000). The galaxies in parenthesis have an unclear classification. The \* are targets analysed both with the new data and in M11.

Core-halo (12+8)	Disky (9+6)	Dusty (3+5)	Bubble (9+13)
IC 1459†	NGC 0841	NGC 3226†	NGC 0266
NGC 0315†	NGC 2681†	NGC 3607†	NGC 0404†
NGC 0410	NGC 2841†	NGC 3627†	NGC 1052†
NGC 2639†	NGC 3185	NGC 3628	NGC 2685
NGC 2787†	NGC 3507	NGC 4125	NGC 3245†
NGC 3623†	NGC 3608	NGC 4374†	NGC 3379*†
NGC 3884	NGC 3642	(NGC 5363)	NGC 3414
NGC 3998†	NGC 3898	NGC 5746	NGC 3718†
NGC 4111†	(NGC 4143)	NGC 5866†	NGC 3945
NGC 4261	(NGC 4203)		NGC 4036†
NGC 4278*	NGC 4314†		(NGC 4143)
NGC 4450	NGC 4321		NGC 4192†
NGC 4494	NGC 4457		(NGC 4203)
NGC 4589	NGC 4552†		NGC 4438†
NGC 4698	NGC 4594†		NGC 4459
NGC 4772	NGC 4736†		NGC 4486†
NGC 5055†	NGC 5077		NGC 4579†
NGC 5957	(NGC 5838)		NGC 4596
NGC 6482	(NGC 7331)		NGC 4636†
NGC 7743			NGC 4696
			NGC 4750
			NGC 5005†
			(NGC 5363)
			NGC 5813
			(NGC 5838)
			NGC 5846†
			(NGC 7331)

large enough (as discs or dust lanes) to not depend on pc-scale structures (see Fig. 6). Specifically, the mean extension of the  $H\alpha$  emission within the HST data is  $0.8 \pm 0.3$  kpc, whereas for the ALFOSC/NOT data is  $1.9 \pm 1.3$  kpc.

We compare the ionised gas morphology with the morphological type of the host galaxy (see Table 1) in order to see if there exists any relationship with the  $H\alpha$  emission beyond the possible star-forming regions in the centres of those galaxies. We see no correlations of the morphologies in the data from M11, in the

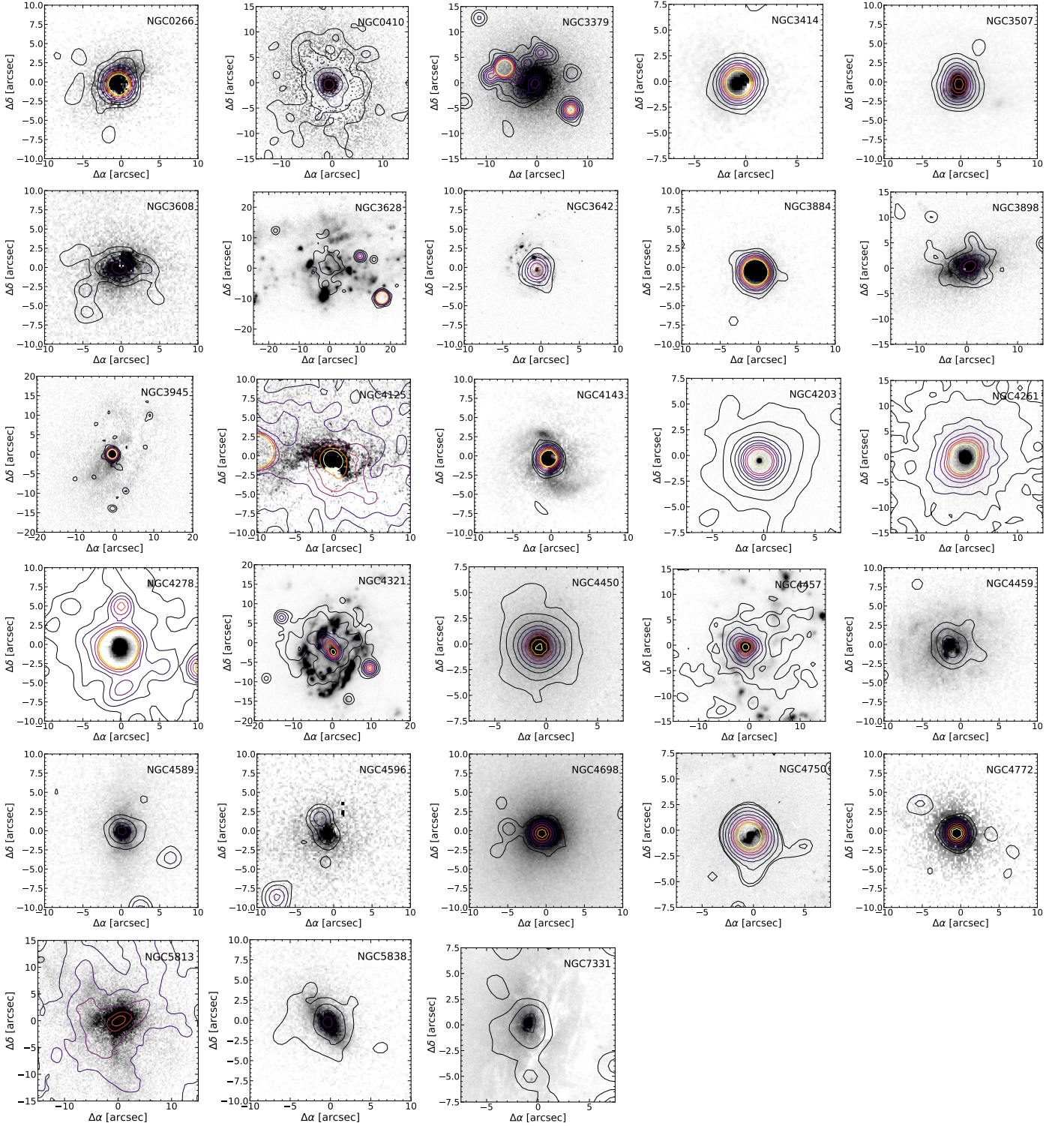


**Fig. 5.**  $H\alpha$  images with overlaid contours of the X-ray emission from Chandra. The contour levels are at  $3\sigma$  (black),  $7\sigma$  (black),  $15\sigma$  (black),  $25\sigma$  (dark-purple),  $40\sigma$  (purple),  $60\sigma$  (light-purple),  $80\sigma$  (red),  $100\sigma$  (orange) and  $150\sigma$  (yellow).

new data, or when considering both together (see Fig. 7). We note that the  $H\alpha$  nuclear emission of all the lenticular galaxies mixing both works was classified as outflow-like, although the sample is small (5 objects) to firmly state any conclusion about it. All the targets are early types, ranging from E to Sb. This is expected, as within the Palomar sample the largest fraction of AGNs (including higher accretion rates) were found among these morphological types (Ho 2008). We find that the major-

ity of galaxies are spirals both in M11 and in this work ( $\sim 60\%$ ; see Fig. 7). This is in contrast to Ho (2008), who stated that for LINERs approximately 35% of the hosts galaxies were ellipticals,  $\sim 45\%$  spirals, while lenticulars were 20%. We selected our LINERs based on their distances (see Table 1) and a previous detection in X-rays that ensured their true nature as AGNs (see Sect. 2 González-Martín et al. 2009). The different selection criteria of the samples may be causing the differing percentages.



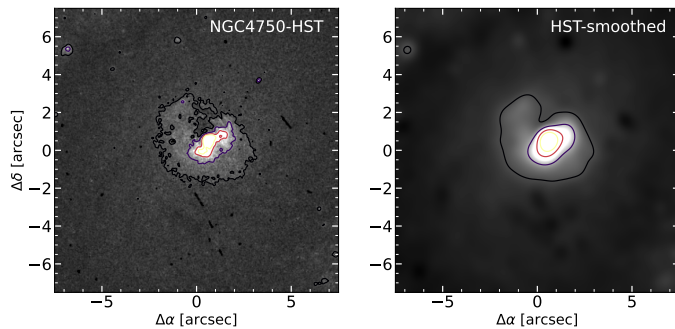


**Fig. 6.** *Left:*  $H\alpha$  emission on NGC 4750 observed with HST (M11). *Right:* Smoothed version of the HST image with a Gaussian filter ( $\sigma \sim 5$ ) to match the ALFOSC/NOT resolution. In both panels, the minimum contour is  $3\sigma$  over the background and the maximum, yellow contour of  $25\sigma$ .

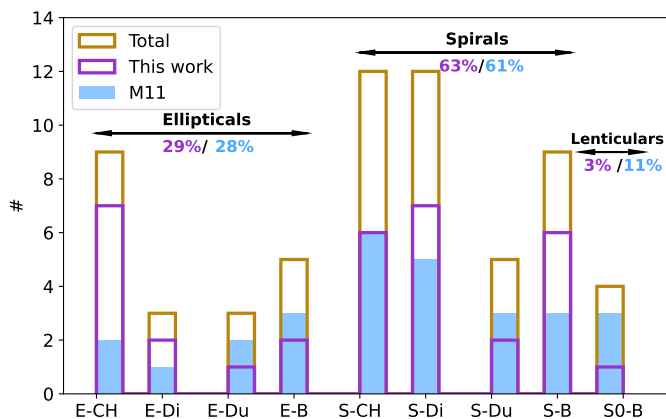


**Fig. 7.** Histogram of the morphological type of the host galaxy and the classification of the nuclear  $H\alpha$  emission. It is divided into ellipticals (E), spirals (S) and lenticulars (S0); ‘CH’ stands for ‘Core-halo’, ‘Di’ for ‘Disky’, ‘Du’ for ‘Dusty’ and ‘B’ for ‘Bubble’. Purple lines indicates the sample from this work; blue for M11; and yellow is the combination of both samples. We have not included unclear cases or irregular galaxies in the figure, and thus the percentages do not sum up 100%.

### 5.1. Outflow candidates with kinematic information

If we take into account all the cases from the sample in this work (see Sect. 4.1), M11 and Pogge et al. (2000), 60 LINERs have spectroscopic data (at least, from long-slit spectroscopy) available in some spectral bands. This information from the literature allows us to estimate the total percentage of kinematically-confirmed (or suggested) outflows in the total sample.

For all the targets classified as ‘Core-halo’, ‘Disky’ and ‘Dusty’ (43 targets) in our  $H\alpha$  data, there is kinematic information available for 33 objects, from which there are reported outflows/inflows in 15, as specified below.

From the 20 classified as ‘Core-halo’, 16 LINERs have kinematical information, and there are outflows reported for 8 LINERs: IC 1459, NGC 0315, NGC 2787, NGC 3884, NGC 3998, NGC 4278, NGC 4450, and NGC 7743. For NGC 0315, NGC 2787 (see also Ruschel-Dutra et al. 2021), NGC 3884, NGC 4278 and NGC 4450 objects the possible outflows (inflow for NGC 4278) were suggested by Cazzoli

et al. (2018) with long-slit spectroscopy of the nuclear region. In IC 1459 the outflow was detected using IFU data from GMOS (Ricci et al. 2014, 2015), although the gas is associated to accretion from the surrounding galaxies with MUSE data in Mulcahey et al. (2021). For NGC 3998 there were hints of non rotational motions in Cazzoli et al. (2018), that were compatible with the perturbed kinematics of the [O III] emission using IFU data of the ATLAS3D survey (Boardman et al. 2017). For NGC 7743 there was an outflow detected in molecular gas using SINFONI (Davies et al. 2014), and several kinematical components detected in the ionised gas studied by Katkov et al. (2011).

In the case of the 15 LINERs classified as ‘Disky’, there is kinematical data for 13 targets. There are outflows/inflows reported only for 4 objects: NGC 2841, NGC 3642, NGC 4594 and NGC 5077. For NGC 2841, Schmidt et al. (2016) detected a small inflow of HI gas, although it is not clear if is caused by gas accretion or minor mergers. For NGC 3642 and NGC 4594 the outflows were detected with long-slit spectroscopy by Cazzoli et al. (2018) and Hermosa Muñoz et al. (2020), respectively. For NGC 5077 there is MUSE IFS data studied in detail by Raimundo (2021), who reports an outflow with the morphology of a hollow cone. The extended ionised emission corresponding to the outflow in that work is similar to what we find at larger scales (see Fig. 4).

From the 8 targets classified as ‘Dusty’, 6 of them have kinematical information in the literature. Outflows have been reported for 4 LINERs: NGC 3226 (Cazzoli et al. 2018), NGC 3627 (inflow in Casasola et al. 2011), NGC 3628 and NGC 5866 (Li 2015). The case of NGC 3628 was already mentioned in Sect. 4.1. There are two hints of outflows in this galaxy (see individual comments in Appendix A), a kpc-scale  $H\alpha$  plume (see Fig. 4) detected in various wavelength bands (Fabbiano et al. 1990; Tsai et al. 2012; Cicone et al. 2014; Fluetsch et al. 2019), and a sub-kpc outflow reported in CO emission (Tsai et al. 2012; Cicone et al. 2014; Roy et al. 2016), that is not visible in our  $H\alpha$  data due to obscuration from the dust lane (it is in the north direction at  $\leq 20''$  from the centre).

From the 22 LINERs classified as ‘Bubble’ (see Sect. 4.1 and Table 4), there is kinematical information available for 21 targets, from which 10 have kinematically detected outflows with either IFS or long-slit spectroscopy. For 13 LINERs, namely NGC 0266, NGC 0404, NGC 1052, NGC 2685, NGC 3379, NGC 3414, NGC 4459, NGC 4486, NGC 4579, NGC 4596, NGC 4696, NGC 5813 and NGC 5846, there is IFS data available (see individual comments on each galaxy in Appendix A, in Pogge et al. 2000 and M11). The IFS data provided hints for non-rotational motions in the velocity maps which could be associated to outflows only for 6 objects, namely NGC 0404, NGC 1052, NGC 3379, NGC 4486, NGC 4579 and NGC 4696. NGC 0404 images show extended  $H\alpha$  emission ascribed to gas blown out possibly by starburst processes (Pogge et al. 2000), that is shown in Nyland et al. (2017) along with the central soft X-ray emission, which have similar extensions, suggesting the presence of shocks. This galaxy was suggested to have outflows associated to a small jet driven by the AGN using ALMA CO(2-1) data (Nyland et al. 2017), although the same emission was also ascribed to supernovae processes (Pogge et al. 2000; Boehle et al. 2018). NGC 1052 was in-depth studied with IFS data, with all the works confirming an outflow in ionised gas (Dopita et al. 2015; Dahmer-Hahn et al. 2019, Cazzoli et al. in prep.). For NGC 3379 the outflow is detected with SAURON data in Shapiro et al. (2006). For NGC 4486 they are mentioned

in Hermosa Muñoz et al. (2020), although the emission is defined as ionised gas filaments with unclear nature in López-Cobá et al. (2020); Sánchez et al. (2021). For NGC 4579, the emission is ascribed to an outflow in several works with long-slit spectroscopy (Walsh et al. 2008; Davies et al. 2014; Mazzalay et al. 2014; Balmaverde & Capetti 2014; Molina et al. 2018), although within the NUGA project, there was an inflow detected in molecular gas, affecting on different galactic scales (García-Burillo et al. 2009; Casasola et al. 2011). For the remaining 7 objects, although there is disturbed gas, it is usually ascribed to past mergers or dust lanes that produce asymmetries in the gas velocities. For NGC 4696, Canning et al. (2011) analysed VIMOS/VLT IFU data, finding a filamentary structure with at least two different kinematic components, probably caused due to interactions with the powerful radio jet and with other members of its galaxy cluster. NGC 2685 has a complex structure: a polar ring blended with an outer ring (see Appendix. A). It was studied with long-slit spectra in previous works (Eskridge & Pogge 1997; Józsa et al. 2009; Hermosa Muñoz et al. 2020), but the different slits were not oriented in the direction of the possible outflow. Boardman et al. (2017) studied its [O III] emission with the ATLAS<sup>3D</sup> survey, finding perturbed kinematics likely not produced by mergers, but by gas accretion of unclear origin. For the other 8 galaxies with bubble-like morphology there is only long-slit spectroscopic data available in the literature. There are outflows reported for 4 targets: NGC 3245 (in Walsh et al. 2008, although not confirmed in Hermosa Muñoz et al. 2020), NGC 4036 (in Walsh et al. 2008, although not confirmed in Cazzoli et al. 2018), NGC 4750 (as an asymmetry in the emission due to dust lanes and spiral arms emerging from the centre Carollo et al. 2002; Cazzoli et al. 2018) and NGC 5005 (from both space and ground-data in Cazzoli et al. 2018) using long-slit spectroscopy. For the other 4 objects there are no outflows detected (NGC 3718, NGC 3945, NGC 4438 and NGC 4636). However, NGC 4438 has an interesting morphological structure (see Fig. 2 in M11). A clear bubble emerging from the nucleus is seen in H $\alpha$  (M11), although the slit was in a direction of the possible outflow in the study by Cazzoli et al. (2018). The nature of this structure would be analysed with IFS data (Hermosa Muñoz et al. in prep.).

There are 5 galaxies whose morphologies were classified as ‘Unclear’. There is kinematical information in the literature for 4 of them (NGC 4143, NGC 4203, NGC 5838, and NGC 7331), where 3 have reported outflows. For NGC 4143 there is only long-slit spectra available, from which the existence of outflows was suggested (Cazzoli et al. 2018). For NGC 4203, NGC 5838 and NGC 7331, there is resolved kinematical information available in the literature (see Appendix A). NGC 4203 is included in the ATLAS<sup>3D</sup> survey, and the HI shows non-rotational motions and inner dust lanes. HI data from the THINGS survey for NGC 7331 (Schmidt et al. 2016) indicated the presence of inflowing/outflowing emission, also suggested in previous works (Mediavilla et al. 1997; Battaner et al. 2003). Finally, for NGC 5838 there are not reported outflows. The IFS data comes from the SAURON survey (Falcón-Barroso et al. 2003; Sarzi et al. 2006), and although they detect asymmetries in the velocity maps, they ascribe them to dust in the nucleus.

Summarising, the kinematic information available for 60 LINERs indicates that there are a total of 29 objects (48%) for which the presence of outflows/inflows was either found or suggested by means of spectroscopic data. Their H $\alpha$  morphology is classified here as ‘Core-halo’, ‘Disky’, ‘Dusty’ or ‘Bubble’, be-

**Table 5.** Percentages of the galaxies with kinematically confirmed outflows in the literature depending on their morphological classification of the H $\alpha$  nuclear emission (see Sect. 5.1 and Appendix A for the comments on individual targets).

Morphological class	Kinematical outflows	Targets
Core-halo	50%	8 (out of 16)
Disky	31%	4 (out of 13)
Dusty	66%	4 (out of 6)
Bubble	48%	10 (out of 21)
Unclear	75%	3 (out of 4)
All classes	48%	29 (out of 60)

ing 3 of them classified as ‘Unclear’ (see Table 4 and Sect. 4.1). The derived percentage is larger to the percentage derived from imaging data (32%, see Sect. 4.3). In Table 5 we have estimated the percentage of kinematically-identified outflows for the morphological classes derived in this work. The percentages in Table 5 indicate that, on average, 1 of every 2 LINERs in the nearby Universe may host an outflow. However, we note that we lack of kinematical information for 10 LINERs in the whole sample of 70, thus the rate may actually vary from 41% up to 56% LINERs with outflows.

Table 5 shows that among the classes with the largest number of objects (>10), the two categories with the largest percentages are ‘Core-halo’ and ‘Bubble’ (50% and 48%, respectively). The objects classified as ‘Disky’ show the lowest percentage within our classification (31%); this could be a matter of the outflow orientation and the inclination of the disc, that may challenge a possible outflow detection (see Sect. 5.3), specially in these low accretion rates where they are expected to be faint. The fraction of LINERs with kinematically confirmed outflows that are morphologically classified as ‘Bubble’-like emission is 34% (10 out of 29). This implies that for the majority of the detected outflows, the ionised gas morphology does not show evident features of a bubble-like emission.

If only IFS data are considered for the identification of kinematical outflows (30 objects with IFS data; see Table 6), only 15 have detected outflows (50%). Small numbers preclude a separate analysis by morphological class, since all but ‘Bubble’ morphologies have IFS data for less than 10 objects. There are 13 objects with IFS information between the ‘Bubble’-like morphologies, among which 6 (46%) show kinematical evidences of outflows, a slightly larger rate than that of the morphological detection (32%).

## 5.2. Soft X-ray / Ionised-gas relationship

It is noticeable that the H $\alpha$  morphologies and the soft X-ray emission are coincident in a large fraction of the new data (~30%), as is the case also for the targets analysed in M11. This behaviour has been seen previously for type-2 Seyferts (Bianchi et al. 2006), where the [O III] and the soft X-ray emission correlated. The work by Bianchi et al. (2019) suggested that Seyferts and LINERs do have similarities in their narrow line regions (see also Pogge et al. 2000), which could lead to the conclusion that these two emissions are produced within the same region of the AGN, and thus a correlation should be expected also in LINERs. The correspondence of the ionised gas morphological signatures, the kinematic results and the X-ray emission for all the galaxies for which we could retrieve data (56 targets: 28 from new data; see Sect. 3) is in Table 6.



M11 performed a similar analysis with the objects from their sample. They gathered data for a total of 28 LINERs in both soft and hard X-rays using Chandra, 4 of which were NGC 3379, NGC 4278, NGC 4676A and B (thus we consider here 24 objects). The results were that, generally, the soft X-ray emission traced that of the ionised gas, and they were correlated in all but 4 galaxies, that seemed to deviate from that trend (NGC 3226, NGC 4486, NGC 5846 and NGC 5866). From all the galaxies with X-ray data in their sample, 20 out of 24 (~83%) showed a correlation in the emission.

By taking into account the new data in this work (see Sect. 4.2), from the 52 objects with soft X-ray data available in the Chandra archive, 31 of them (60%; see Table 6) do show a correlation with the ionised gas emission. According to our results (see Table 6), 29 targets have reported outflows or inflows with kinematical information. Only 12 LINERs (namely IC 1459, NGC 2787, NGC 2841, NGC 3245, NGC 3884, NGC 3998, NGC 4036, NGC 4450, NGC 4579, NGC 4594, NGC 4696 and NGC 4750) have both features simultaneously, that is 23% (12 over 52). However, the reported outflows in all the objects but 5 (IC 1459, NGC 2841, NGC 3998, NGC 4579 and NGC 4696) come from long-slit spectroscopy. As discussed previously (see Sect. 5), although useful, these spectra do not fully characterise the AGN and its environment, given the spatial limitations of the technique. This combined with the small number of coincidences, do not allow to draw any firm conclusion about a possible correlation between the presence of an outflow and an extended X-ray emission.

### 5.3. Comparison with other active galaxies

So far, there are two systematic searches of outflows in LINERs with both ground and space-based long-slit spectroscopic data. These were done by Cazzoli et al. (2018) and Hermosa Muñoz et al. (2020), who analysed 22 (type-1) and 9 (type-2) LINERs, finding an outflow detection-rate of 41% and 22%, respectively. Considering the sample number, the rate of outflows we report in this study (48%) is in agreement with that by Cazzoli et al. (2018).

There are several works searching for outflows in the nearby Universe for different active galaxies in different wavelength ranges (Cazzoli et al. 2016; Fiore et al. 2017; Fluetsch et al. 2019, 2021; Ruschel-Dutra et al. 2021), and also at higher redshifts (e.g. Harrison et al. 2016,  $0.6 \leq z \leq 1.7$ , with ~50% kinematic detections of ionised outflows). Within the kinematical data from the literature gathered in this work with LINERs in the Local Universe, not all the targets with kinematically-identified outflows are based on ionised gas (19 out of 29 in ionised gas). There are evidences for extended outflows on different spatial scales (from sub-kpc to several kpc), associated to both AGNs and starburst activity (Veilleux et al. 2005, e.g. M 82, see Leroy et al. 2015). Luo et al. (2021) studied the ionised emission for 40 nearby ( $z < 0.1$ ) type-2 AGNs, finding a correlation between the outflow sizes and the [O III] luminosities. The typical sizes of the kinematically-identified outflows varied from 0.9 to 4 kpc (median 2 kpc), which are similar sizes to those quoted by previous works (e.g. mean of 1.8 kpc for luminous  $z < 1$  AGNs in Bae et al. 2017; 0.1 to 3 kpc for 6 Seyfert-2 galaxies in Revalski et al. 2021). In this work we focus on the circumnuclear emission of the galaxies as it is expected that the possible outflows are less intense in LINERs. However, the  $H\alpha$  emission in our images has similar extensions, with a mean observed size of 1.9 kpc, rang-

ing in all morphologies from 0.2 to 6 kpc (0.5 to ~2 kpc for only the bubble-like morphologies).

Concas et al. (2019), by exploiting SDSS spectra, suggested that although the inclination of the host galaxy is crucial to detect the outflowing emission, if the ionised outflows are AGN-driven and the accretion disc is not connected to the host disc, then the outflow may be launched in another direction, not perpendicular to the host. Fischer et al. (2013) obtained the inclination of the AGN in 17 Seyfert galaxies, finding that the biconical outflows were more easily detected in those that were type-2 AGNs (i.e. oriented edge-on). From our imaging data and the kinematic analysis from the literature, we find that inclination could be important, as the lowest percentages of outflows are in ‘Disky’ systems (e.g. NGC 4321). Given that the intensity of the outflowing gas scales with the activity of the AGN (Fluetsch et al. 2019; Revalski et al. 2021), and that their extension is typically ~1 kpc (one of the largest seen with our images is NGC 3945 ~1.5 kpc; see Fig. B.4), we could be missing outflows due to inclination effects. As already noticed by Fischer et al. (2013), these effects are potentially more relevant for close to face-on targets in which the outflow has a cone-like shape, as the inclination effects may lead to misleading morphological classifications. Within our sample, between the kinematically-detected outflows there are 19 type-1 (5 IFS, 14 LSS) and 10 type-2 LINERs (8 IFS, 2 LSS)<sup>3</sup>. Those detected with long-slit spectroscopy are only nuclear outflows. Curiously, for the IFS outflowing detections in type-1s, the typical sizes are larger than 1 kpc (i.e. ~1 kpc for NGC 1052, ~2.3 kpc for NGC 4696, ~5 kpc for IC 1450), whereas for type-2s the sizes are usually detected on a sub-kpc scale (i.e. ~40 pc NGC 0404 or ~700 pc for NGC 7743). This would be expected based on the unified model, as type-2 LINERs are oriented edge-on and thus outflows oriented in the polar direction would be more easily detected than on more face-on type-1 LINERs.

## 6. Summary and conclusions

In this work we present a morphological analysis of 70 nearby LINERs with both ALFOSC/NOT and HST narrow band imaging corresponding to the  $H\alpha$  emission. We have obtained new data for a total of 38 galaxies, whereas the remaining 32 come from previous works (Pogge et al. 2000, M11). The  $H\alpha$  imaging data indicate that among these AGNs there is a variety of morphologies within the ionised gas, that can be classified in 4 different groups, as in M11, plus an additional class for objects with an ambiguous classification.

The statistics derived from the total sample of 70 LINERs suggest that ~32% of LINERs have bubble-like ionised gas morphologies, ~29% show compact circumnuclear emission (‘Core-halo’) and ~21% have emission associated to the disc or the spiral arms of the host galaxy. For ~11% of the sample we cannot state anything on the morphologies, as there is nuclear dust preventing from obtaining a complete vision of the ionised gas. Additionally, the complex distribution of the gas in ~7% of the sample lead us to an unclear classification of the sources based exclusively on imaging information. However, there is kinematical information in the literature for 80% (4 out of 5) of these sources with ‘Unclear’ morphology that provides more evidences on the possible origin of the emission (see Sect. 5.1).

<sup>3</sup> The distribution of type-1 and type-2 LINERs in the complete sample is 38% and 62% respectively (based on Ho et al. 1997; Cazzoli et al. 2018; Hermosa Muñoz et al. 2020)

**Table 6.** Galaxies with available X-ray data and its correspondence with the morphological signatures in  $H\alpha$  and the kinematically-confirmed outflows or inflows in the literature (see Sect. 5.1, Sect. 5.2 and Fig. 5). In column (2) we include the morphological classification according to Sect. 4. Column (3) indicates whether the spectral information was obtained with long-slit spectroscopy (LSS) or IFS. In column (4) and (5): ‘Y’ stands for Yes and ‘N’ for No. Column (4) indicates if the X-ray emission is co-spatial with the  $H\alpha$  morphology (see Sect. 4.2). Targets from Pogge et al. (2000) and Masegosa et al. (2011) are marked with †.

Galaxy (1)	Morphology (2)	Spectra (3)	Outflow/Inflow (4)	X-ray (5)	Galaxy (1)	Morphology (2)	Spectra (3)	Outflow/Inflow (4)	X-ray (5)
NGC 0266	Bubble	IFS	N	Y	NGC 4698	Core-halo	IFS	N	N
NGC 0404 <sup>†</sup>	Bubble	IFS	Y	-	NGC 4772	Core-halo	IFS	N	Y
NGC 1052 <sup>†</sup>	Bubble	IFS	Y	-	NGC 5055 <sup>†</sup>	Core-halo	IFS	N	Y
NGC 2685	Bubble	IFS	N	-	NGC 5957	Core-halo	-	-	-
NGC 3245 <sup>†</sup>	Bubble	LSS	Y	Y	NGC 6482	Core-halo	LSS	N	-
NGC 3379	Bubble	IFS	Y	N	NGC 7743	Core-halo	IFS	Y	-
NGC 3414	Bubble	IFS	N	Y					
NGC 3718 <sup>†</sup>	Bubble	LSS	N	-	NGC 0841	Disky	LSS	N	-
NGC 3945	Bubble	LSS	N	Y	NGC 2681 <sup>†</sup>	Disky	LSS	N	Y
NGC 4036 <sup>†</sup>	Bubble	LSS	Y	Y	NGC 2841 <sup>†</sup>	Disky	IFS	Y	Y
NGC 4192 <sup>†</sup>	Bubble	-	-	-	NGC 3185	Disky	-	-	-
NGC 4438 <sup>†</sup>	Bubble	LSS	N	Y	NGC 3507	Disky	IFS	N	N
NGC 4459	Bubble	IFS	N	N	NGC 3608	Disky	IFS	N	N
NGC 4486 <sup>†</sup>	Bubble	IFS	Y	N	NGC 3642	Disky	LSS	Y	N
NGC 4579 <sup>†</sup>	Bubble	IFS	Y	Y	NGC 3898	Disky	LSS	N	N
NGC 4596	Bubble	IFS	N	Y	NGC 4314 <sup>†</sup>	Disky	-	-	Y
NGC 4636 <sup>†</sup>	Bubble	LSS	N	Y	NGC 4321	Disky	IFS	N	N
NGC 4696 <sup>†</sup>	Bubble	IFS	Y	Y	NGC 4457	Disky	IFS	N	N
NGC 4750	Bubble	LSS	Y	Y	NGC 4552 <sup>†</sup>	Disky	LSS	N	Y
NGC 5005 <sup>†</sup>	Bubble	LSS	Y	-	NGC 4594 <sup>†</sup>	Disky	LSS	Y	Y
NGC 5813	Bubble	IFS	N	Y	NGC 4736 <sup>†</sup>	Disky	LSS	N	Y
NGC 5846 <sup>†</sup>	Bubble	IFS	N	N	NGC 5077	Disky	IFS	Y	-
IC 1459 <sup>†</sup>	Core-halo	IFS	Y	Y	NGC 3226 <sup>†</sup>	Dusty	LSS	Y	N
NGC 0315 <sup>†</sup>	Core-halo	LSS	Y	N	NGC 3607 <sup>†</sup>	Dusty	-	-	Y
NGC 0410	Core-halo	IFS	N	Y	NGC 3627 <sup>†</sup>	Dusty	IFS	Y	-
NGC 2639 <sup>†</sup>	Core-halo	-	-	-	NGC 3628	Dusty	IFS	Y	N
NGC 2787 <sup>†</sup>	Core-halo	LSS	Y	Y	NGC 4125	Dusty	-	-	N
NGC 3623 <sup>†</sup>	Core-halo	-	-	-	NGC 4374 <sup>†</sup>	Dusty	LSS	N	Y
NGC 3884	Core-halo	LSS	Y	Y	NGC 5746	Dusty	IFS	N	-
NGC 3998 <sup>†</sup>	Core-halo	IFS	Y	Y	NGC 5866 <sup>†</sup>	Dusty	LSS	Y	N
NGC 4111 <sup>†</sup>	Core-halo	-	-	Y					
NGC 4261	Core-halo	IFS	N	Y	NGC 4143	Unclear	LSS	Y	N
NGC 4278	Core-halo	LSS	Y	N	NGC 4203	Unclear	IFS	Y	N
NGC 4450	Core-halo	LSS	Y	Y	NGC 5363	Unclear	-	-	-
NGC 4494	Core-halo	IFS	N	-	NGC 5838	Unclear	IFS	N	Y
NGC 4589	Core-halo	LSS	N	N	NGC 7331	Unclear	IFS	Y	N

Considering all the kinematic information available, accounting for both long-slit and IFS data, we have data for 60 LINERs. The statistics evidence that 48% of the objects do show outflow kinematic signatures (see Sect. 5.1). This percentage is somewhat larger than that derived from the morphological signatures (32%). Since we still miss kinematic information for 10 targets of the 70 LINERs, the total rate could vary from 41% up to 56% LINERs with outflows. With the complete morphological and kinematical information combined, we find that at least 1 out of every 3 nearby ( $z < 0.025$ ) LINERs may have a galactic outflow, probably associated to the activity of the super massive black hole, given that they are mainly detected in ionised gas.

The morphological signatures combined with the kinematical information suggest that, considering our number statistics, it is equally probable to find an outflow in a LINER in which the ionised gas morphology is bubble-like than if it is core-halo-like (see Sect. 5.1).

We found evidences that the soft X-ray emission follows that from the ionised gas in 31 LINERs (~60% above the total with X-ray data) from the galaxies analysed in this work. This means that for the majority of targets there is a correlation between the ionised  $H\alpha$  gas and the soft X-ray, as it was proposed in previous works for higher-luminosity AGNs (Bianchi et al. 2006, 2019). Both emissions are then expected to be raised in the same spatial region of the AGN. We note though that the results may vary and that we could find (or not) a strong correlation between the emissions as we still lack soft X-ray data for a 25% of the sample (i.e. 18 LINERs). Specifically, the correlation percentage may vary up to 70% (44%) if both emissions are (not) co-spatial for all the remaining targets. We do not see any correlation between the spectroscopically-confirmed outflows and the co-spatiality of these emissions (ionised gas and soft X-rays). Therefore, with the data that we have, we can say that the soft X-ray emission is not a strong predictor of the presence of kinematically evident outflows. As for the  $H\alpha$  imaging, considering all the kinematical information available, our results suggest that

those objects with Disky-like structures have less probability of hosting an outflow, probably due to the orientation, whereas for the remaining morphologies, the probability of detection is 55%.

*Acknowledgements.* We thank the anonymous referee for his/her very constructive comments that have helped to improve the paper. We acknowledge financial support from the Spanish Ministerio de Ciencia, Innovación y Universidades (MCIU) under the grants AYA2016-76682-C3 and PID2019-106027GB-C41. Authors acknowledge financial support from the State Agency for Research of the Spanish MCIU through the ‘Centre of Excellence Severo Ochoa’ award to the Instituto de Astrofísica de Andalucía (SEV-2017-0709). LHM acknowledge financial support under the grant BES-2017-082471.

The data presented here were obtained in part with ALFOSC, which is provided by the Instituto de Astrofísica de Andalucía (IAA) under a joint agreement with the University of Copenhagen and NOTSA. This work is based on observations made with the NASA/ESA Hubble Space Telescope, and obtained from the Hubble Legacy Archive, which is a collaboration between the Space Telescope Science Institute (STScI/NASA), the Space Telescope European Coordinating Facility (ST-ECF/ESA) and the Canadian Astronomy Data Centre (CADAC/NRC/CSA). This research has made use of data obtained from the Chandra Data Archive and software provided by the Chandra X-ray Centre in the application package CIAO.

This research has made use of the NASA/IPAC Extragalactic Database (NED), which is operated by the Jet Propulsion Laboratory, California Institute of Technology, under contract with the National Aeronautics and Space Administration. We acknowledge the usage of the HyperLeda database (<http://leda.univ-lyon1.fr>).

This work has made extensive use of IRAF (v2.16) and Python (v3.8.10), particularly with ASTROPY (v4.2, <http://www.astropy.org>; Astropy Collaboration et al. 2013, 2018), MATPLOTLIB (v3.4.1; Hunter 2007), PHOTUTILS (v1.1.0; Bradley et al. 2020) and NUMPY (v1.19.4; Harris et al. 2020).

Authors acknowledge M. Guerrero and B. Pérez for their help in some observing runs, and the support astronomers at the NOT telescope that made the observations during service time.

## References

- Afanasyev, V. L. & Silchenko, O. K. 2007, *Astronomical and Astrophysical Transactions*, 26, 311
- Allard, E. L., Peletier, R. F., & Knapen, J. H. 2005, *ApJ*, 633, L25
- Arsenault, R., Roy, J. R., & Boulesteix, J. 1990, *A&A*, 234, 23
- Astropy Collaboration, Price-Whelan, A. M., Sipőcz, B. M., et al. 2018, *AJ*, 156, 123
- Astropy Collaboration, Robitaille, T. P., Tollerud, E. J., et al. 2013, *A&A*, 558, A33
- Bacon, R., Copin, Y., Monnet, G., et al. 2001, *MNRAS*, 326, 23
- Baldi, R. D., Rodríguez Zaurín, J., Chiaberge, M., et al. 2019, *ApJ*, 870, 53
- Balmaverde, B. & Capetti, A. 2014, *A&A*, 563, A119
- Barentine, J. C. & Kormendy, J. 2012, *ApJ*, 754, 140
- Battaner, E., Mediavilla, E., Gujarro, A., Arribas, S., & Florido, E. 2003, *A&A*, 401, 67
- Bertola, F., Corsini, E. M., Beltrán, J. C. V., et al. 1999, *ApJ*, 519, L127
- Bianchi, S., Guainazzi, M., & Chiaberge, M. 2006, *A&A*, 448, 499
- Bianchi, S., Guainazzi, M., Laor, A., Stern, J., & Behar, E. 2019, *MNRAS*, 485, 416
- Boardman, N. F., Weijmans, A.-M., van den Bosch, R., et al. 2017, *MNRAS*, 471, 4005
- Boehle, A., Larkin, J. E., Armus, L., & Wright, S. A. 2018, *ApJ*, 866, 79
- Boizelle, B. D., Walsh, J. L., Barth, A. J., et al. 2021, *ApJ*, 908, 19
- Bradley, L., Sipőcz, B., Robitaille, T., et al. 2020, *astropy/photutils: 1.0.0*
- Braun, R., Oosterloo, T. A., Morganti, R., Klein, U., & Beck, R. 2007, *A&A*, 461, 455
- Brodie, J. P., Romanowsky, A. J., Strader, J., et al. 2014, *ApJ*, 796, 52
- Canning, R. E. A., Fabian, A. C., Johnstone, R. M., et al. 2011, *MNRAS*, 417, 3080
- Carollo, C. M., Franx, M., Illingworth, G. D., & Forbes, D. A. 1997, *ApJ*, 481, 710
- Carollo, C. M., Stiavelli, M., Seigar, M., de Zeeuw, P. T., & Dejonghe, H. 2002, *AJ*, 123, 159
- Casasola, V., Hunt, L. K., Combes, F., García-Burillo, S., & Neri, R. 2011, *A&A*, 527, A92
- Cazzoli, S., Arribas, S., Colina, L., et al. 2014, *A&A*, 569, A14
- Cazzoli, S., Arribas, S., Maiolino, R., & Colina, L. 2016, *A&A*, 590, A125
- Cazzoli, S., Gil de Paz, A., Márquez, I., et al. 2020, *MNRAS*, 493, 3656
- Cazzoli, S., Márquez, I., Masegosa, J., et al. 2018, *MNRAS*, 480, 1106
- Cepa, J. & Beckman, J. E. 1990, *A&AS*, 83, 211
- Chemin, L., Balkowski, C., Cayatte, V., et al. 2006, *MNRAS*, 366, 812
- Chiaraluce, E., Bruni, G., Panessa, F., et al. 2019, *MNRAS*, 485, 3185
- Cicone, C., Maiolino, R., Sturm, E., et al. 2014, *A&A*, 562, A21
- Combes, F., Young, L. M., & Bureau, M. 2007, *MNRAS*, 377, 1795
- Concas, A., Popesso, P., Brusa, M., Mainieri, V., & Thomas, D. 2019, *A&A*, 622, A188
- Corsini, E. M., Méndez-Abreu, J., Pastorello, N., et al. 2012, *MNRAS*, 423, L79
- Corsini, E. M., Morelli, L., Zarattini, S., et al. 2018, *A&A*, 618, A172
- Cortés, J. R., Kenney, J. D. P., & Hardy, E. 2015, *ApJS*, 216, 9
- Cresci, G. & Maiolino, R. 2018, *Nature Astronomy*, 2, 179
- Dahmer-Hahn, L. G., Riffel, R., Ricci, T. V., et al. 2019, *MNRAS*, 489, 5653
- Davies, R., Baron, D., Shimizu, T., et al. 2020, *MNRAS*, 498, 4150
- Davies, R. I., Maciejewski, W., Hicks, E. K. S., et al. 2014, *ApJ*, 792, 101
- Davis, T. A. & McDermid, R. M. 2017, *MNRAS*, 464, 453
- Díaz-García, S., Moyano, F. D., Comerón, S., et al. 2020, *A&A*, 644, A38
- Dopita, M. A., Ho, I.-T., Dressel, L. L., et al. 2015, *ApJ*, 801, 42
- Dopita, M. A. & Sutherland, R. S. 1995, *ApJ*, 455, 468
- Dullo, B. T., Martínez-Lombilla, C., & Knapen, J. H. 2016, *MNRAS*, 462, 3800
- Emsellem, E., Cappellari, M., Peletier, R. F., et al. 2004, *MNRAS*, 352, 721
- Ene, I., Ma, C.-P., Veale, M., et al. 2018, *MNRAS*, 479, 2810
- Ene, I., Ma, C.-P., Walsh, J. L., et al. 2020, *ApJ*, 891, 65
- Epinat, B., Amram, P., & Marcelin, M. 2008, *MNRAS*, 390, 466
- Erroz-Ferrer, S., Knapen, J. H., Mohd Noh Velastín, E. A. N., Ryon, J. E., & Hagen, L. M. Z. 2013, *MNRAS*, 436, 3135
- Erwin, P. & Debattista, V. P. 2017, *MNRAS*, 468, 2058
- Erwin, P., Pohlen, M., & Beckman, J. E. 2008, *AJ*, 135, 20
- Erwin, P. & Sparke, L. S. 1999, *ApJ*, 521, L37
- Eskridge, P. B. & Pogge, R. W. 1997, *ApJ*, 486, 259
- Fabbiano, G., Heckman, T., & Keel, W. C. 1990, *ApJ*, 355, 442
- Fabian, A. C. 2012, *ARA&A*, 50, 455
- Falcón-Barroso, J., Bacon, R., Bureau, M., et al. 2006, *MNRAS*, 369, 529
- Falcón-Barroso, J., Balcells, M., Peletier, R. F., & Vazdekis, A. 2003, *A&A*, 405, 455
- Filho, M. E., Barthel, P. D., & Ho, L. C. 2002, *ApJS*, 142, 223
- Finkelman, I., Brosch, N., Funes, J. G., Kniazev, A. Y., & Väisänen, P. 2010, *MNRAS*, 407, 2475
- Fiore, F., Feruglio, C., Shankar, F., et al. 2017, *A&A*, 601, A143
- Fischer, T. C., Crenshaw, D. M., Kraemer, S. B., & Schmitt, H. R. 2013, *ApJS*, 209, 1
- Fluetsch, A., Maiolino, R., Carniani, S., et al. 2021, *MNRAS*, 505, 5753
- Fluetsch, A., Maiolino, R., Carniani, S., et al. 2019, *MNRAS*, 483, 4586
- Forbes, D. A. 1996, *AJ*, 112, 1409
- Foster, C., Spitler, L. R., Romanowsky, A. J., et al. 2011, *MNRAS*, 415, 3393
- García-Burillo, S., Fernández-García, S., Combes, F., et al. 2009, *A&A*, 496, 85
- García-Burillo, S., Sempere, M. J., Combes, F., & Neri, R. 1998, *A&A*, 333, 864
- Gerssen, J., Kuijken, K., & Merrifield, M. R. 1999, *MNRAS*, 306, 926
- González Delgado, R. M., Pérez, E., Cid Fernandes, R., & Schmitt, H. 2008, *AJ*, 135, 747
- González-Martín, O., Masegosa, J., Márquez, I., & Guainazzi, M. 2009, *ApJ*, 704, 1570
- González-Martín, O., Masegosa, J., Márquez, I., Guainazzi, M., & Jiménez-Bailón, E. 2009, *A&A*, 506, 1107
- Goudfrooij, P., Hansen, L., Jorgensen, H. E., & Norgaard-Nielsen, H. U. 1994a, *A&AS*, 105, 341
- Goudfrooij, P., Hansen, L., Jorgensen, H. E., et al. 1994b, *A&AS*, 104, 179
- Hameed, S. & Devereux, N. 2005, *AJ*, 129, 2597
- Harris, C. R., Millman, K. J., van der Walt, S. J., et al. 2020, *Nature*, 585, 357
- Harrison, C. M., Alexander, D. M., Mullaney, J. R., et al. 2016, *MNRAS*, 456, 1195
- Haynes, M. P., Jore, K. P., Barrett, E. A., Broeils, A. H., & Murray, B. M. 2000, *AJ*, 120, 703
- Heckman, T. M. 1980, *A&A*, 87, 152
- Hermosa Muñoz, L., Cazzoli, S., Márquez, I., & Masegosa, J. 2020, *A&A*, 635, A50
- Ho, L. C. 2008, *ARA&A*, 46, 475
- Ho, L. C., Filippenko, A. V., & Sargent, W. L. W. 1997, *ApJS*, 112, 315
- Hunter, J. D. 2007, *Computing in Science & Engineering*, 9, 90
- James, P. A. & Percival, S. M. 2016, *MNRAS*, 457, 917
- Józsa, G. I. G., Oosterloo, T. A., Morganti, R., Klein, U., & Erben, T. 2009, *A&A*, 494, 489
- Kaneda, H., Ishihara, D., Onaka, T., et al. 2011, *PASJ*, 63, 601
- Katkov, I. Y., Moiseev, A. V., & Sil’chenko, O. K. 2011, *ApJ*, 740, 83
- Kent, S. M. 1990, *AJ*, 100, 377
- Knapen, J. H., Cepa, J., Beckman, J. E., Soledad del Rio, M., & Pedlar, A. 1993, *ApJ*, 416, 563
- Knapen, J. H., Shlosman, I., Heller, C. H., et al. 2000, *ApJ*, 528, 219
- Koopmann, R. A. & Kenney, J. D. P. 2006, *ApJS*, 162, 97
- Koopmann, R. A., Kenney, J. D. P., & Young, J. 2001, *ApJS*, 135, 125
- Kormendy, J. 1979, *ApJ*, 227, 714

- Kormendy, J. 1984, *ApJ*, 287, 577
- Kormendy, J. & Ho, L. C. 2013, *ARA&A*, 51, 511
- Krajnović, D., Weillbacher, P. M., Urrutia, T., et al. 2015, *MNRAS*, 452, 2
- Kuo, C.-Y., Lim, J., Tang, Y.-W., & Ho, P. T. P. 2008, *ApJ*, 679, 1047
- Lakhchaura, K., Werner, N., Sun, M., et al. 2018, *MNRAS*, 481, 4472
- Laurikainen, E. & Salo, H. 2017, *A&A*, 598, A10
- Laurikainen, E., Salo, H., Buta, R., & Knapen, J. H. 2011, *MNRAS*, 418, 1452
- Leroy, A. K., Schinnerer, E., Hughes, A., et al. 2021, arXiv e-prints, arXiv:2104.07739
- Leroy, A. K., Walter, F., Martini, P., et al. 2015, *ApJ*, 814, 83
- Li, J.-T. 2015, *MNRAS*, 453, 1062
- López-Cobá, C., Sánchez, S. F., Anderson, J. P., et al. 2020, *AJ*, 159, 167
- Luo, R., Woo, J.-H., Karouzos, M., et al. 2021, *ApJ*, 908, 221
- Ma, C.-P., Greene, J. E., McConnell, N., et al. 2014, *ApJ*, 795, 158
- Márquez, I., Durret, F., González Delgado, R. M., et al. 1999, *A&AS*, 140, 1
- Márquez, I., Masegosa, J., Durret, F., et al. 2003, *A&A*, 409, 459
- Márquez, I., Masegosa, J., González-Martín, O., et al. 2017, *Frontiers in Astronomy and Space Sciences*, 4, 34
- Márquez, I. & Moles, M. 1989, *A&AS*, 120, 1
- Masegosa, J., Márquez, I., Ramirez, A., & González-Martín, O. 2011, *A&A*, 527, A23
- Mazzalay, X., Maciejewski, W., Erwin, P., et al. 2014, *MNRAS*, 438, 2036
- Mediavilla, E., Arribas, S., García-Lorenzo, B., & del Burgo, C. 1997, *ApJ*, 488, 682
- Mingozzi, M., Cresci, G., Venturi, G., et al. 2019, *A&A*, 622, A146
- Moellenhoff, C. & Bender, R. 1989, *A&A*, 214, 61
- Molaeinezhad, A., Falcón-Barroso, J., Martínez-Valpuesta, I., et al. 2016, *MNRAS*, 456, 692
- Molina, M., Eracleous, M., Barth, A. J., et al. 2018, *ApJ*, 864, 90
- Morganti, R. 2017, *Frontiers in Astronomy and Space Sciences*, 4, 42
- Mosenkov, A., Rich, R. M., Koch, A., et al. 2020, *MNRAS*, 494, 1751
- Mulcahey, C. R., Prichard, L. J., Krajnović, D., & Jorgenson, R. A. 2021, *MNRAS*, 504, 5087
- Nemmen, R. S., Storchi-Bergmann, T., & Eracleous, M. 2014, *MNRAS*, 438, 2804
- Nyland, K., Davis, T. A., Nguyen, D. D., et al. 2017, *ApJ*, 845, 50
- Osterbrock, D. E. & Ferland, G. J. 2006, *Astrophysics of gaseous nebulae and active galactic nuclei*, 2nd. ed. by D.E. Osterbrock and G.J. Ferland. Sausalito, CA: University Science Books, 2006
- Pagotto, I., Corsini, E. M., Sarzi, M., et al. 2019, *MNRAS*, 483, 57
- Pandya, V., Greene, J. E., Ma, C.-P., et al. 2017, *ApJ*, 837, 40
- Peters, W. & Kuzio de Naray, R. 2017, *MNRAS*, 469, 3541
- Pignatelli, E., Corsini, E. M., Vega Beltrán, J. C., et al. 2001, *MNRAS*, 323, 188
- Pogge, R. W., Maoz, D., Ho, L. C., & Eracleous, M. 2000, *ApJ*, 532, 323
- Pu, S. B., Saglia, R. P., Fabricius, M. H., et al. 2010, *A&A*, 516, A4
- Raimundo, S. I. 2021, *A&A*, 650, A34
- Ramos Almeida, C. & Ricci, C. 2017, *Nature Astronomy*, 1, 679
- Randall, S. W., Forman, W. R., Giacintucci, S., et al. 2011, *ApJ*, 726, 86
- Randall, S. W., Nulsen, P. E. J., Jones, C., et al. 2015, *ApJ*, 805, 112
- Rest, A., van den Bosch, F. C., Jaffe, W., et al. 2001, *AJ*, 121, 2431
- Revalski, M., Meena, B., Martinez, F., et al. 2021, *ApJ*, 910, 139
- Ricci, T. V., Steiner, J. E., & Menezes, R. B. 2014, *MNRAS*, 440, 2419
- Ricci, T. V., Steiner, J. E., & Menezes, R. B. 2015, *MNRAS*, 451, 3728
- Roy, A., Nath, B. B., Sharma, P., & Shchekinov, Y. 2016, *MNRAS*, 463, 2296
- Ruschel-Dutra, D., Storchi-Bergmann, T., Schnorr-Müller, A., et al. 2021, *MNRAS*, 507, 74
- Sakamoto, K., Okumura, S., Minezaki, T., Kobayashi, Y., & Wada, K. 1995, *AJ*, 110, 2075
- Sánchez, S. F., Walcher, C. J., Lopez-Cobá, C., et al. 2021, *Rev. Mexicana Astron. Astrofis.*, 57, 3
- Sánchez-Gallego, J. R., Knapen, J. H., Wilson, C. D., et al. 2012, *MNRAS*, 422, 3208
- Sarzi, M., Falcón-Barroso, J., Davies, R. L., et al. 2006, *MNRAS*, 366, 1151
- Sarzi, M., Shields, J. C., Schawinski, K., et al. 2010, *MNRAS*, 402, 2187
- Scarlata, C., Stiavelli, M., Hughes, M. A., et al. 2004, *AJ*, 128, 1124
- Schmidt, T. M., Bigiel, F., Klessen, R. S., & de Blok, W. J. G. 2016, *MNRAS*, 457, 2642
- Shapiro, K. L., Cappellari, M., de Zeeuw, T., et al. 2006, *MNRAS*, 370, 559
- Sharp, R. G. & Bland-Hawthorn, J. 2010, *ApJ*, 711, 818
- Storchi-Bergmann, T., Schimoia, J. S., Peterson, B. M., et al. 2017, *ApJ*, 835, 236
- Trinchieri, G., Pellegrini, S., Fabbiano, G., et al. 2008, *ApJ*, 688, 1000
- Tsai, A.-L., Matsushita, S., Kong, A. K. H., Matsumoto, H., & Kohno, K. 2012, *ApJ*, 752, 38
- Ulrich, M.-H. 1975, *PASP*, 87, 965
- van den Bosch, F. C., Ferrarese, L., Jaffe, W., Ford, H. C., & O'Connell, R. W. 1994, *AJ*, 108, 1579
- Veilleux, S., Cecil, G., & Bland-Hawthorn, J. 2005, *ARA&A*, 43, 769
- Veilleux, S., Maiolino, R., Bolatto, A. D., & Aalto, S. 2020, *A&A Rev.*, 28, 2
- Walsh, J. L., Barth, A. J., Ho, L. C., et al. 2008, *AJ*, 136, 1677
- Watkins, A. E., Mihos, J. C., Harding, P., & Feldmeier, J. J. 2014, *ApJ*, 791, 38
- Wild, V., Rosales-Ortega, F., Falcón-Barroso, J., et al. 2014, *A&A*, 567, A132
- Wilson, C. D., Cridland, A., Foyle, K., et al. 2013, *ApJ*, 776, L30
- Yıldız, M. K., Peletier, R. F., Duc, P. A., & Serra, P. 2020, *A&A*, 636, A8
- Young, L. M., Bureau, M., & Cappellari, M. 2008, *ApJ*, 676, 317

## Appendix A: Individual comments on galaxies

*NGC 0266* (see Fig. B.1): The  $H\alpha$  emission of this barred galaxy was studied by Epinat et al. (2008). These authors obtained the velocity maps with data from the GHASP survey, finding gas with disturbed morphology, that could be consistent with past interactions. Considering all the regions with  $H\alpha$  emission of NGC 0266 (out to  $\sim 2'$ ), we only find emission along the spiral arms and extended in the centre (see upper panel of Fig. B.1). In the work by Epinat et al. (2008), they detected additional gas distributed along the major axis of the galaxy, following the spiral arms but also randomly distributed, with large voids of gas near the centre.

*NGC 0410* (see Fig. B.1): It belongs to a small group of galaxies together with NGC0407 and NGC0414 (non-active systems). We have classified the emission of this object as 'Core-halo' (see Table 4). No extended  $H\alpha$  emission has been reported previously (Lakhchaura et al. 2018). This galaxy is also included in the MASSIVE survey (Ma et al. 2014), but only the stellar kinematics is shown (Ene et al. 2020).

*NGC 0841* (see Fig. B.1): González Delgado et al. (2008) characterised this galaxy as hosting a nuclear spiral and a dust lane using F547M HST imaging. Our sharp-divided image also suggests a ring-like nuclear structure. The  $H\alpha$  image shows strong emission in the nucleus and clumpy emission regions along the disc, probably associated to multiple star forming regions. Thus, we classified it as 'Disky'. The HI data of this system show a perturbed morphology indicative of its interaction with NGC 0834 (not in this sample), located south-east of our galaxy, although both systems are optically undisturbed (Kuo et al. 2008). In fact, the ionised and neutral gas of this galaxy follow a rotation pattern (Cazzoli et al. 2018).

*NGC 2685* (see Fig. B.1): This galaxy shows a complex structure, hosting an inner, polar ring and an outer ring, proposed to correspond to a warped disc, oriented as the galaxy disc (Józsa et al. 2009). The HI gas morphology is disturbed with the presence of non-circular motions (likely due to the interaction between these two different rings), although its rotation curve is nearly that of a spiral (Józsa et al. 2009). Boardman et al. (2017) studied the [O III] kinematics for this galaxy within the ATLAS<sup>3D</sup> survey, finding a disturbed velocity map, probably ascribed to gas accretion. In Hermosa Muñoz et al. (2020) the long-slit spectrum analysed shows very narrow line profiles ( $\sigma \sim 65 \text{ kms}^{-1}$ ) in both space- and ground-based spectra, although neither was oriented in the direction in which we see an extended ionised emission ( $\text{PA} \sim 120^\circ$ ; see middle-down panel in Fig. B.1). This asymmetric emission coming from the nucleus, extending up to 10 arcsec, was also pointed out by Ulrich (1975) using long-slit spectroscopy around the [O II] $\lambda 3727\text{\AA}$  line. Eskridge & Pogge (1997) obtained optical spectroscopy to study the H II regions of the galaxy and  $H\alpha$  imaging data where they traced the nuclear emission, stating that the asymmetry probably is produced due to extinction effects. In our work we

ascribe this emission to the possible presence of an outflow, probably not detected kinematically due to the orientation of the slit (e.g. PA=38° and 54° in Hermosa Muñoz et al. 2020).

*NGC 3185* (see Fig. B.2): We have classified the ionised gas emission of this galaxy as ‘Disky’, with a clear unresolved nuclear structure that was proposed to be a ring in several works (James & Percival 2016; Laurikainen & Salo 2017), coincident with the radio emission in Chiaraluce et al. (2019). In these works the nature of the ring is ascribed to a bar that is driven star formation in the nucleus. Laurikainen & Salo (2017) also supports that view, finding an ‘X-shape’ in their image, usually present in barred galaxies. On the contrary, Díaz-García et al. (2020) defines the nuclear enhanced star forming region not as a ring, but as a circumnuclear starburst for NGC 3185.

*NGC 3379* (see Fig. B.2): We classified the ionised gas in this galaxy as ‘Bubble’, as we found evidence for extended H $\alpha$  emission with an elongated shape in the innermost parts of the image ( $\sim 4''$ ). This substructure (PA $\sim 41^\circ$ ) is spatially coincident with a nuclear dust lane at a PA $\sim 50^\circ$  (Masegosa et al. 2011). Watkins et al. (2014) also found extended emission when studying this galaxy. The H $\alpha$  emission shows no particular asymmetric structures and no evidences of any previous merger interactions. When they apply a elliptical fitting to the brightness profile, their residuals show an ‘X’-like shape, just as seen in our SD image (see Fig. B.2), usually present in barred systems. Trinchieri et al. (2008) discovered the presence of outflowing emission near the centre with a width of  $\sim 800$  pc (larger than the apparent width in our H $\alpha$  image  $\sim 300$  pc) with deep soft X-ray Chandra observations. Using kinematic data, Shapiro et al. (2006) obtained information within the SAURON sample of the stellar and gaseous component of this galaxy. They found a regular rotating gas disc and also evidences of non-rotational motions.

*NGC 3414* (see Fig. B.2): This is a peculiar S0 galaxy, with a faint disc over a prominent bulge (Koopmann & Kenney 2006). In our images, the H $\alpha$  morphology is classified as an ‘Bubble’. Our results show the nuclear emission with a non-symmetric shape that could be due to the presence of dust in the south-west direction, as previously reported. Specifically, the analysis in the R band with HST data done by Rest et al. (2001) suggest the presence of dust in the nucleus. This is also confirmed by Koopmann & Kenney (2006), as they found centrally concentrated ionised gas distorted by the presence of dust. Sarzi et al. (2006) studied this galaxy using SAURON data, finding a spiral pattern in the gas distribution, that was generally rotating perpendicularly to the stellar component.

*NGC 3507* (see Fig. B.2): We have classified the ionised gas morphology of this galaxy as ‘Disky’. Previous H $\alpha$  imaging from the literature (Sánchez-Gallego et al. 2012) trace the large scale ionised gas distribution that is also seen in our images, but with worse seeing (theirs  $1.3''$  vs ours  $1.0''$ ). The CO map from the PHANGS-ALMA survey, which provides the CO(2-1) line emission at about  $1''$  resolution (Leroy et al. 2021), traces molecular gas along the dust-lanes seen in the sharp-divided images, broadly resembling the ionised gas emission. A detailed analysis of the CO kinematics would reveal whether the atomic gas is participating from the putative outflow indicated by the H $\alpha$  morphology.

*NGC 3608* (see Fig. B.3): We have classified the H $\alpha$  morphology of this galaxy as ‘Disky’. Similarly, Goudfrooij et al. (1994a) found the distribution of ionised gas to be nearly face-on and symmetric, with no evidences of dust absorption. Afanasiev & Silchenko (2007) found evidences of the ionised gas rotating perpendicular to the stars, with complex stellar kinematics (counter rotating components). They found no evidences of outflows, although they do see a strong variation of the gas photometric and kinematic major axes at  $\sim 1-4$  arcsec from the nucleus, that would indicate the presence of polar gas rotation. They claim the existence of a inclined gaseous ring of  $\sim 200$  pc, which would be coincident with the inner contours of our H $\alpha$  image. This galaxy was observed within the ATLAS3D sample, but the weakness of the measured emission lines avoid any kinematical analysis.

*NGC 3628* (see Fig. B.3): The nuclear emission in this galaxy is classified as ‘Dusty’ given the large amount of dust that prevents from seen the galactic centre. At larger scales (up to  $100''$ ) Fabbiano et al. (1990) reported for the first time the presence of an outflow in this galaxy, based on H $\alpha$  observations, reporting that it is coincident with an X-ray plume. This work was latter supported by several other studies in other wavelength bands. Specifically, Tsai et al. (2012) reported the existence of is a sub-kpc scale outflow north of the disc, detected with CO(1-0) emission, expanding at  $50 \text{ km s}^{-1}$  outwards of the galaxy. This was confirmed by Cicone et al. (2014) using also molecular gas observations, and they mention that this outflow is spatially coincident with a large scale plasma outflow ( $\sim 10$  kpc) that was detected with soft X-ray observations with Chandra. The outflow studied by Tsai et al. (2012) is described as being a weak bubble coming through a central and larger outflow (Roy et al. 2016). Sharp & Bland-Hawthorn (2010) observed this galaxy with the AAOmega IFS, finding filamentary emission and outflowing gas, with evidences of large-scale shocks. We also see signatures of a large scale outflow in our data, out of the dust lane (up to  $\sim 80''$ ), seen in Fig. 4.

*NGC 3642* (see Fig. B.3): As in our image, Pogge et al. (2000) detect a strong nuclear source surrounded by some diffuse circumnuclear H $\alpha$  emission. We have classified this emission as ‘Disky’, concentrated along the spiral arms, with no outflowing signatures. Scarlata et al. (2004) describe the nuclear region of this galaxy as being elongated, probably due to a dust lane, from where dusty spiral arms emerge. The kinematic study performed by Cazzoli et al. (2018) suggest the presence of two kinematic components in the nuclear spectrum, being the broadest component a candidate signature of a nuclear outflow.

*NGC 3884* (see Fig. B.3): The H $\alpha$  morphology of our image shows a rather elongated structure along the galaxy disc (see last row of Fig. B.3); we classified it as ‘Core-halo’. The soft X-ray emission is coincident with the ionised gas (see Fig. 5). Despite the simple distribution of the ionised gas, in Cazzoli et al. (2018) they modelled the emission lines of the ionised gas with two kinematic components. The broadest component is blueshifted and was interpreted as a possible nuclear outflow.

*NGC 3898* (see Fig. B.4): In our image we find that the distribution of the H $\alpha$  gas is extended and Disky. This is consistent with previous works as Hameed & Devereux (2005) with data from the CCD imager of the Kitt Peak National Observatory, or Pignatelli et al. (2001), using imaging data from the Vatican Advanced Technology Telescope and spectra from the Isaac

Newton Telescope. This latter work found that the distribution of the ionised gas is smooth within the bulge of the galaxy, but rather clumpy within the disc, due to the presence of H II regions. From this work, we can infer from the distribution of these regions that both the gas and stellar components are coincident in the same plane. On the contrary Carollo et al. (2002) reported an irregular nuclear emission with strong dust component with data from NICMOS/HST. They found red nuclear emission with elongated features, surrounded by a large scale disc or bar-like structure connected with a spiral feature north-east from the nucleus.

*NGC 3945* (see Fig. B.4): In our H $\alpha$  image we see clear hints of filamentary emission (up to  $\sim 15''$ ), which we have classified as ‘Bubble’. This emission could be co-spatial with some internal features mentioned in previous works such as a pseudo-bulge (R $\sim 4''$  Kormendy 1979), two bars (R $\sim 2-3''$  Erwin & Sparke 1999) or a lens which is coincident with the larger bar (R $\sim 26''$  Dullo et al. 2016). Laurikainen et al. (2011) identified the barlens for the first time oriented along the minor axis of the galaxy, however Erwin & Debattista (2017) stated that instead that feature resembles to be associated to a larger inner/nuclear disc.

*NGC 4125* (see Fig. B.4): This elliptical galaxy contains a disc (e.g. van den Bosch et al. 1994; Goudfrooij et al. 1994b) and filamentary nuclear dust (e.g. Goudfrooij et al. 1994a; Braun et al. 2007), visible in our sharp-divided image, that lead us to a ‘Dusty’ morphological classification. This galaxy is not detected with radio emission (Filho et al. 2002), HI or CO gas (Wilson et al. 2013). The soft-X rays are much more extended and not correlated with the ionised gas, that is however correlated with the PAH emission (Kaneda et al. 2011). Pu et al. (2010) obtained the long slit spectrum of the nucleus, finding evidences of rotation along both the major and minor axes of the galaxy, and young stellar populations in the centre, which could indicate the existence of material coming from a past merger. They found the ionised gas to be oriented along the major axis of the galaxy (as we see it in our H $\alpha$  image), following non-rotational motions, no ascribed to outflows.

*NGC 4143* (see Fig. B.4): Our H $\alpha$  morphology is classified as ‘Unclear’, given that the image shows extended emission along the galaxy disc, but part of the gas (or even the whole emission) could be associated to a possible outflow (see Cazzoli et al. 2018). The nuclear spectra of this galaxy was studied by Cazzoli et al. (2018) based on TWIN/CAHA observations. They found two kinematic components in the ionised gas, with the broadest component consistent with an outflow.

*NGC 4203* (see Fig. B.5): The ionised gas morphology in our data set is classified as ‘Unclear’, as there is some extended emission that cannot be classified as coming from the disc or from outflowing emission exclusively from imaging data. Yıldız et al. (2020) characterised the object as a spiral-like, HI-rich, dusty galaxy (their Fig. C1), and gave an extinction map oriented east-west, in contrast to the north-south orientation of the H $\alpha$  emission in our image. The nuclear spectrum of this galaxy has complicated profiles with several components (Storchi-Bergmann et al. 2017; Cazzoli et al. 2018). Stellar and gas kinematics from IFU spectroscopy were obtained by Boardman et al. (2017) with the Mitchell spectrograph. The derived gas kinematics, even with sparser spatial resolution, seem to indicate that non-rotational motions, associated to outflows,

could be present roughly along the north-south direction.

*NGC 4261* (see Fig. B.5): The H $\alpha$  emission is concentrated near the nucleus, thus we classified it as ‘Core-halo’. We find a correlation in the orientation of the soft X-ray emission and the ionised gas, although the first is much more extended ( $>15''$  from the centre). Baldi et al. (2019) published H $\alpha$  and [O III] images obtained with HST, showing a notably less extended H $\alpha$  emission (maximum  $3''$  vs our  $\geq 5''$ ) and more asymmetric (more emission to the west) than what we find. Boizelle et al. (2021) used high resolution (about  $0.2''$ ) CO observations with ALMA, finding that the molecular gas extends  $2''$  on both sides along the north-south axis. The molecular gas kinematics can be globally reproduced by a rotating disc model.

*NGC 4278* (see Fig. B.5): This HI-rich (Yıldız et al. 2020), elliptical galaxy hosts a regular disc (Sarzi et al. 2006). The ionised gas morphology is classified here as ‘Core-halo’ as it is centrally concentrated (see also Masegosa et al. 2011). In Cazzoli et al. (2018) the emission lines of the nuclear spectrum show two kinematic components, one of them consistent with an inflow.

*NGC 4321* (see Fig. B.5): This galaxy has been studied in different wavelength bands. Specifically, the ionised gas emission (e.g. Arsenault et al. 1990; Cepa & Beckman 1990; Knapen et al. 2000), the molecular gas (e.g. Sakamoto et al. 1995; Garcia-Burillo et al. 1998) and the HI emission, which is coincident with the optical disc (Knapen et al. 1993). Our H $\alpha$  morphological image is classified as ‘Disky’ as it clearly follows the disc of the galaxy, the separation of the 4 spiral arms and several star forming regions (also visible in molecular gas Garcia-Burillo et al. 1998). The central region was analysed with SAURON IFS data (Allard et al. 2005), that reported an enhancement of the H $\beta$  emission in the ring as well as two dust lanes at the end of the bar of the galaxy. The existence of dust in the disc plane makes the definition of the spiral arms difficult (Scarlata et al. 2004).

*NGC 4450* (see Fig. B.6): This barred spiral galaxy was classified as hosting a truncated star forming disc at  $\sim 60''$  from the nucleus, given the non-continuous H $\alpha$  emission at large scales (Koopmann et al. 2001; Chemin et al. 2006). In the innermost parts of the galaxy (i.e.  $5''$  from the centre) we find the H $\alpha$  emission concentrated in a ‘Core-halo’ morphology. This is in agreement with the image on Koopmann et al. (2001), where the nuclear emission is not extended further out to the galaxy ( $<10''$ ), except for some sparse regions at larger scales ( $\sim 30''$ , i.e.  $\sim 3$  kpc). Cortés et al. (2015) obtained the velocity field for this galaxy, finding two plateaus at a distance  $\sim 5''$  from the centre, that suggested the presence of an additional rotating component. The [O III] emission has an offset of  $25^\circ$  with respect to the main stellar component, that was ascribed to the recent acquisition of gas into the galaxy (Cortés et al. 2015). This additional component is also confirmed by Cazzoli et al. (2018), who detected a secondary component in the forbidden lines, although it was interpreted as outflows/inflows.

*NGC 4457* (see Fig. B.6): This face-on galaxy has many star forming regions, clearly visible in our H $\alpha$  image (classified as ‘Disky’), found only in the inner  $30''$  (Cortés et al. 2015). This galaxy is known to host a radio jet, although the PA is not reported in the literature (see Nemmen et al. 2014, and references therein). Both the stellar and the ionised gas components are

rotating, but non-circular motions have been detected. This is seen in the gas velocity map, that is more disturbed than that of the stars, specially along the stellar kinematic minor axis (Cortés et al. 2015). In our image it is clearly visible an H $\alpha$  arm in the approaching side of the galaxy, as in previous works (Chemin et al. 2006; Cortés et al. 2015). The gas kinematic centre has the most blue-shifted velocities (Chemin et al. 2006), and its centre is not spatially coincident with the stellar kinematic centre (Cortés et al. 2015). In the work by Cortés et al. (2015), they suggest that the arm and the velocity maps of the ionised gas component are indicative of ram pressure stripping effects.

*NGC 4459* (see Fig. B.6): This unbarred lenticular galaxy has an extended dust disc up to  $\sim 8''$  from the nucleus (Pagotto et al. 2019, and references therein). The ionised gas morphology is classified here as ‘Bubble’, as it shows two small blobs south from the nucleus, in the direction of the molecular gas kinematic minor axis (Young et al. 2008). The blobs are not seen in previous kinematic maps of the ionised gas (H $\beta$  line in Sarzi et al. 2006). The H $\alpha$  emission is extended up to  $\sim 10''$  from the nucleus in the west-east direction (in agreement with Koopmann et al. 2001), concentrated in a disc as the H $\beta$  emission (Sarzi et al. 2006, 2010). Various works have studied the molecular gas traced by the CO in the galaxy (Combes et al. 2007; Young et al. 2008; Davis & McDermid 2017) which is detected along an oval shape, similar to that of the H $\alpha$ , coincident with dust lanes (visible in our sharp-divided image, see third, right panel in Fig. B.6). The concentrated molecular gas suggests the existence of ongoing circumnuclear star formation (Sarzi et al. 2006). The kinematic information of the CO (2-1) suggest a regular rotating disc (Davis & McDermid 2017).

*NGC 4494* (see Fig. B.6): This elliptical galaxy is characterised by an inner edge-on dusty ring of star formation (Forbes 1996). So far, our study is the first one focused on the ionised gas of this galaxy. In our image the H $\alpha$  emission shows a ‘Core-halo’ morphology, extended up to  $40''$  from the nucleus (with a  $3\sigma$ -detection). Foster et al. (2011) found a double structure in the global kinematics derived from individual globular clusters, which they ascribe to a recent gas-rich merger, although we do not see any feature of this in the ionised gas. The stellar kinematics was further studied within the ATLAS3D survey (Krajnović et al. 2015) and the SLUGGS survey (Brodie et al. 2014), in which they found a regular rotation pattern, particularly flat in the outer parts of the galaxy.

*NGC 4589* (see Fig. B.7): The ionised gas in this elliptical galaxy shows a ‘Core-halo’ morphology with a dust lane along the minor axis also seen in previous works (Moellenhoff & Bender 1989; Goudfrooij et al. 1994a). Moellenhoff & Bender (1989) performed a spectroscopic study of the object that revealed complex gas and stellar kinematics, with gas moving along several position angles. They associated these motions to a previous merger. This latter event may also have caused the minor-axis dust lane by accretion of external material. The ionised gas is co-spatial with the dust lane as it already settled down, which is consistent with being produced in an old merger (Moellenhoff & Bender 1989).

*NGC 4596* (see Fig. B.7): It is a strong barred galaxy (Kent 1990; Gerssen et al. 1999; Laurikainen & Salo 2017) with a faint dust spiral and a compact source in the nucleus (González Delgado et al. 2008). Our image of the H $\alpha$  emission reveals an outflow-like morphology, with an asymmetric profile with

respect to the nucleus. Falcón-Barroso et al. (2006) studied this galaxy within the SAURON sample (Bacon et al. 2001), mentioning the misalignment in the kinematic and photometric axes of this galaxy, due to a bar. The stellar and gaseous component are aligned, both with a regular rotation pattern. In the SAURON map, the H $\beta$  gas is centrally concentrated (Falcón-Barroso et al. 2006), similar to what we see for H $\alpha$  in our image.

*NGC 4698* (see Fig. B.7): Our H $\alpha$  image has a morphology that we classified as ‘Core-halo’. Erroz-Ferrer et al. (2013) included this object in their sample, where they also obtained H $\alpha$  imaging with ALFOSC/NOT. They were only interested in the double-ring structure seen at large scales, hence the comparison of the nuclear region with the published H $\alpha$  image is not possible. Bertola et al. (1999) reported that the nuclear disc of gas and stars are rotating perpendicularly with respect to the galaxy main disc, most probably as a result of acquisition of external gas (Corsini et al. 2012). Cortés et al. (2015) spatially studied resolved stellar and ionised gas kinematics, and suggested that this Virgo cluster galaxy is the product of an ancient merger. They also concluded that the ionised gas kinematics (traced with [O III] in the central  $5''$ ) is non-planar. In Hermosa Muñoz et al. (2020) the line profiles are narrow ( $\sigma \sim 90 \text{ kms}^{-1}$ ) for both space- and ground-based spectroscopic data.

*NGC 4750* (see Fig. B.7): The morphology of the H $\alpha$  gas of this galaxy, ‘Bubble’, is correlated with the soft X-ray emission (see Sect. 5.2). Carollo et al. (2002) reported the presence of spiral features emerging from the nucleus, stronger in the north-east direction, using NICMOS/HST images. They found evidence of strong dust features and star formation. In our data, specially in the sharp-divided image, we also detect the spiral arms and the presence of dust. However, the gas seems to be outflowing from the nucleus rather than being distributed along the spiral arms, and we do not detect star-forming regions. In Cazzoli et al. (2018) the nuclear spectrum show features of an outflow (broad component in forbidden lines and narrow H $\alpha$ ). Indeed, the slit is oriented towards the outflow detected by our imaging data (PA =  $231^\circ$ ).

*NGC 4772* (see Fig. B.8): The H $\alpha$  emission of this galaxy is classified here as ‘Core-halo’. Haynes et al. (2000) reported a centrally peaked emission surrounded by diffuse gas affected by the presence of a dust lane, coincident with HI gas. They suggest that this galaxy may have gone through a merger that spread out the gas through the disc. Falcón-Barroso et al. (2006) detected ionised gas with SAURON data that was oriented in the north-west and south-west direction, possibly coming from a ring out of the main galactic plane. Although there could be other interpretations as the main stellar and gas components of this galaxy are known to co-rotate. In our image we detect a nuclear source both in the ionised and soft X-ray emissions, that is diffuse and extended for H $\alpha$  in the same direction as in Falcón-Barroso et al. (2006).

*NGC 5077* (see Fig. B.8): In our image the H $\alpha$  gas seems to follow the galactic spiral arms or disc; thus we classified it as a ‘Disky’ morphology. The analysis of MUSE IFS data by Raimundo (2021) confirmed the presence of a stellar distinct, counter-rotating core with complex gas dynamics. In fact, our H $\alpha$  distributions are very similar. She reports the discovery of a nuclear outflow, consistent with a hollow cone intersecting the



plane of the sky.

*NGC 5363* (see Fig. B.8): The galaxy is classified as I0 in NED database, although the images may contradict this classification due to an inner spiral structure (Finkelman et al. 2010). In our  $H\alpha$  image this internal structure is seen, as in Finkelman et al. (2010), although is not detected in the R broad-band image. This galaxy shows an internal dust lane that obscures the nuclear emission, and extends further out from the nucleus (Finkelman et al. 2010). No outflow/inflow signatures are seen neither in the sharp-divided image nor in the pure  $H\alpha$  image in the nuclear region. However, at larger scales in our image there is extended emission, whose nature is not clear. This lead to our classification as ‘Unclear’.

*NGC 5746* (see Fig. B.8): This is an edge-on, quiescent spiral galaxy, with no evidences of recent mergers (Barentine & Kormendy 2012; Mosenkov et al. 2020). Our image shows a heavily obscured nucleus due to a dust lane that prevents from seeing the nuclear  $H\alpha$  emission. Integral field spectroscopy is reported only for the extraction of the stellar kinematics, from which the presence of a bar is determined (Molaeinezhad et al. 2016; Peters & Kuzio de Naray 2017).

*NGC 5813* (see Fig. B.9): The most notable feature of this elliptical is that it hosts a kinematically decoupled core (Kormendy 1984; Krajnović et al. 2015). Carollo et al. (1997) reported the presence of a dust lane along the major axis of the galaxy, stating that the dust itself may be suggesting the existence of the two reported cores. Our image of the ionised gas reveals that is very extended emission (see Fig. 4) with filamentary structures that resemble an outflow. In previous  $H\alpha$  observations with the Imager on the SOAR telescope, Randall et al. (2011) reported the presence of filaments co-spatial with the radio emission and with cool gas. They also reported that part of the central  $H\alpha$  emission is anti-correlated with some inner X-rays cavities, although we do find a rough correlation with the soft X-ray emission. With MUSE IFU data, Krajnović et al. (2015) identified two counter-rotating components (visible in the emission lines) and a disturbed velocity dispersion in the stellar component. The  $H\alpha$ -[N II] emission revealed the presence of knots and filaments along the polar direction of the galaxy, also visible in our image. Both lines have a uniform velocity dispersion and both approaching and receding velocities with respect to the systemic velocity of the galaxy (Krajnović et al. 2015). The origin of this emission is explained in Krajnović et al. (2015) as being related to the X-rays cavities and the jet activity, due to the interaction of the gas filaments with the plasma, being a gas reservoir of the galaxy rather than an inflow or an outflow. Despite its complex kinematics and its double nucleus, this galaxy is not believed to have gone through a major merger (Randall et al. 2015).

*NGC 5838* (see Fig. B.9): This is an inclined lenticular galaxy ( $i = 72^\circ$ , see Table. 1), with a thin bar (Molaeinezhad et al. 2016; Laurikainen & Salo 2017), fast, regular disc rotation (Emsellem et al. 2004). There is reported minor axis rotation, probably produced by asymmetry effects in the velocity maps due to the presence of a nuclear dust disc (Falcón-Barroso et al. 2003). This dust disc is subtle, but visible in our broad-band image. Our narrow-band image precludes to interpret if the gas is lying in the galaxy disc or it may be produced by outflowing processes given its asymmetry. Sarzi et al. (2006) found a regular dust disc and a relatively small scale of the gas distribution (maximum

extension up to  $\sim 10''$  north-east from the nucleus), being  $H\beta$  similar to our  $H\alpha$  distribution. These authors remarked its similarity with NGC 4459, both in the gas distribution and in the kinematic maps, whose ionised gas we classified here as an ‘Bubble’ (see individual comments for that galaxy).

*NGC 5957* (see Fig. B.9): This galaxy has previous observations with the NOT telescope in the broad R filter, studied in the work by Erwin et al. (2008). However, they could not determine all their properties due to problems with the sky subtraction. Similarly, our observations of this galaxy suffered from poor sky conditions and high clouds (see Sect. 2), which is translated into a flux loss; we cannot state anything about the ionised gas morphology beyond the pure nuclei, due to the low signal-to-noise.

*NGC 6482* (see Fig. B.9): This galaxy is the brightest object of its fossil group (Corsini et al. 2018). The ionised gas in our image has a ‘Core-halo’ morphology. The object was studied in the context of the MASSIVE survey (Ma et al. 2014), were Ene et al. (2018) found a regular rotation pattern in the stellar component, well aligned with the photometric axis. They found that it is one of the galaxies with more warm gas from the sample, extended up to 16 kpc, in contrast to the ionised gas that goes up to 4 kpc. They associated it to cooling flows that may be connected to the X-ray emission in the system (Pandya et al. 2017). Corsini et al. (2018) analysed the stellar and gaseous components of the galaxy via long-slit spectroscopy, finding a young stellar population that may have been produced by a recent merger or AGN feedback processes.

*NGC 7331* (see Fig. B.10): This is a highly inclined spiral galaxy ( $i = 72^\circ$ , see Table 1) located in a group along other 4 galaxies (NGC 7335, NG 7336, NGC 7337, and NGC 7340). The  $H\alpha$  gas is asymmetric, resembling an outflow-like morphology. Mediavilla et al. (1997) studied the ionised gas emission, in particular the [O III] lines, that were modelled with 3 different components associated to: systemic velocity, a blueshifted component and a redshifted component. They interpret the components as coming from a disc and a shell of gas, although they do not discard the presence of an outflow/inflow. Battaner et al. (2003) suggest the existence of a massive stellar formation ring, through which there is infalling matter into the inner regions of the galaxy. Inflowing and outflowing material in this galaxy were also found using HI data from the THINGS survey (Schmidt et al. 2016).

*NGC 7743* (see Fig. B.10): We have classified the ionised gas morphology as ‘Core-halo’. The analysis of both long-slit and IFS spectroscopic data made by Katkov et al. (2011) conclude that the ionised gas present several components in the inner  $1-2''$ , one of them probably produced by the interaction of the jet from the AGN with the ambient interstellar medium. This could be related to what we see in our image, that the  $H\alpha$  contours in that regions shows a slightly different orientation than the outer contours (north-south vs northeast-southwest). The  $H_2$  velocity field derived from K-band IFS with SINFONI allowed Davies et al. (2014) to conclude that the molecular gas is outflowing from the AGN.

## Appendix B: $H\alpha$ and sharp-divided images



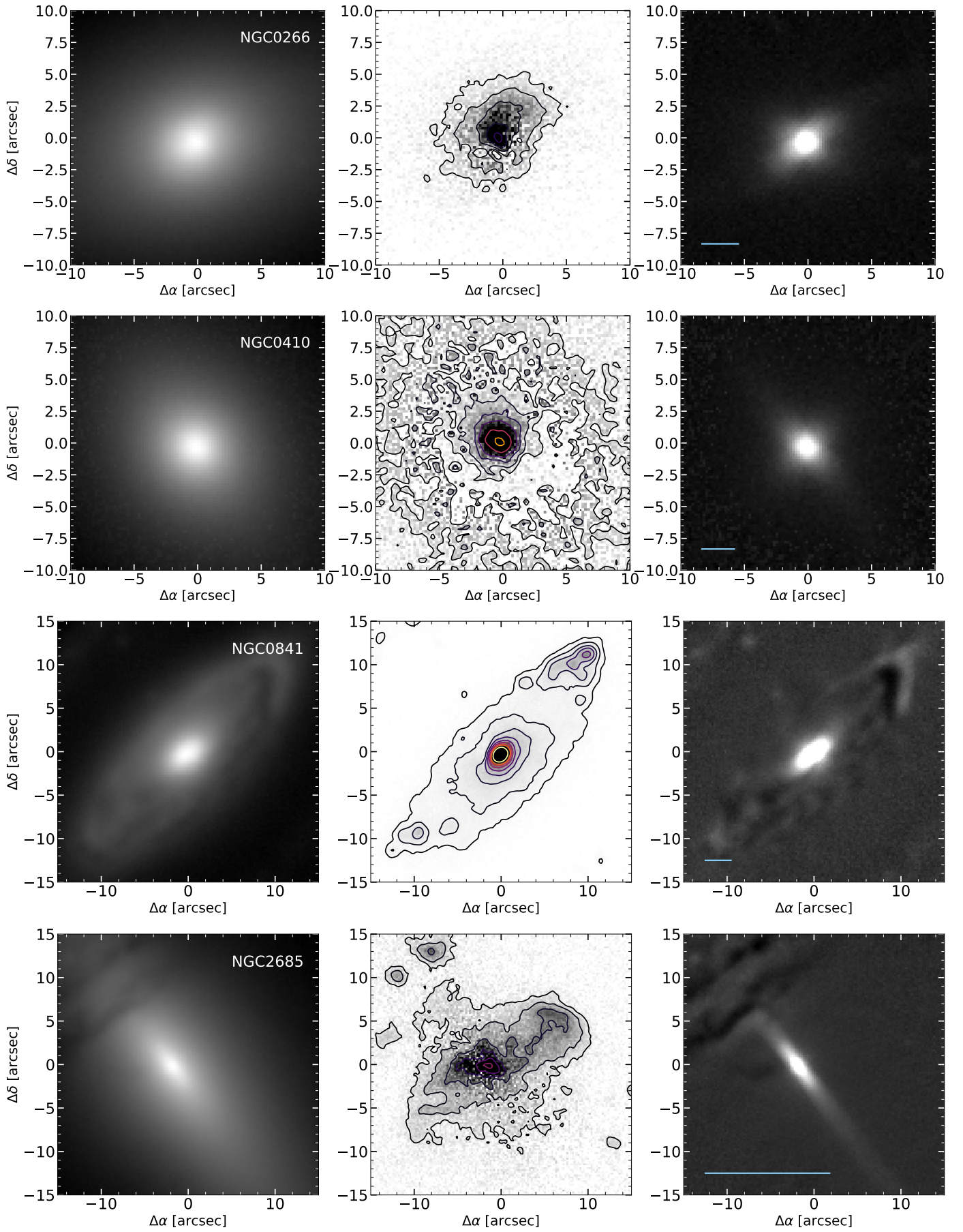


**Fig. B.1.** *Left:* Original NF image. *Middle:*  $H\alpha$  image of NGC 0266, NGC 0410, NGC 0841 and NGC 2685 with contours at  $3\sigma$  (black),  $7\sigma$  (black),  $15\sigma$  (black),  $25\sigma$  (dark-purple),  $40\sigma$  (purple),  $60\sigma$  (light-purple),  $80\sigma$  (red),  $100\sigma$  (orange) and  $150\sigma$  (yellow) levels. *Right:* Sharp-divided BF image. The blue line indicates the 1 kpc scale.

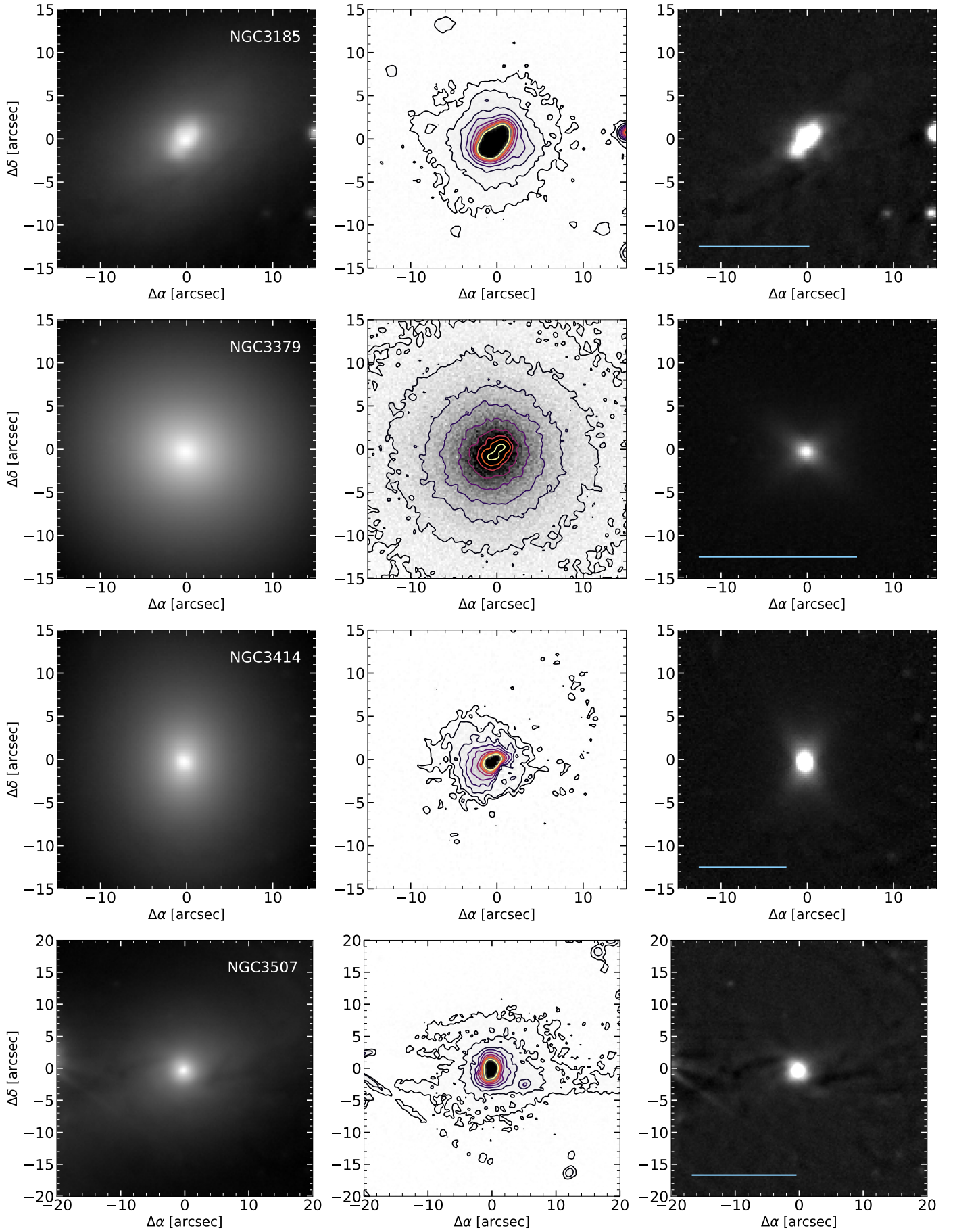


**Fig. B.2.** NGC 3185, NGC 3379, NGC 3414 and NGC 3507  $H\alpha$  emission. The complete description is in Fig. B.1.

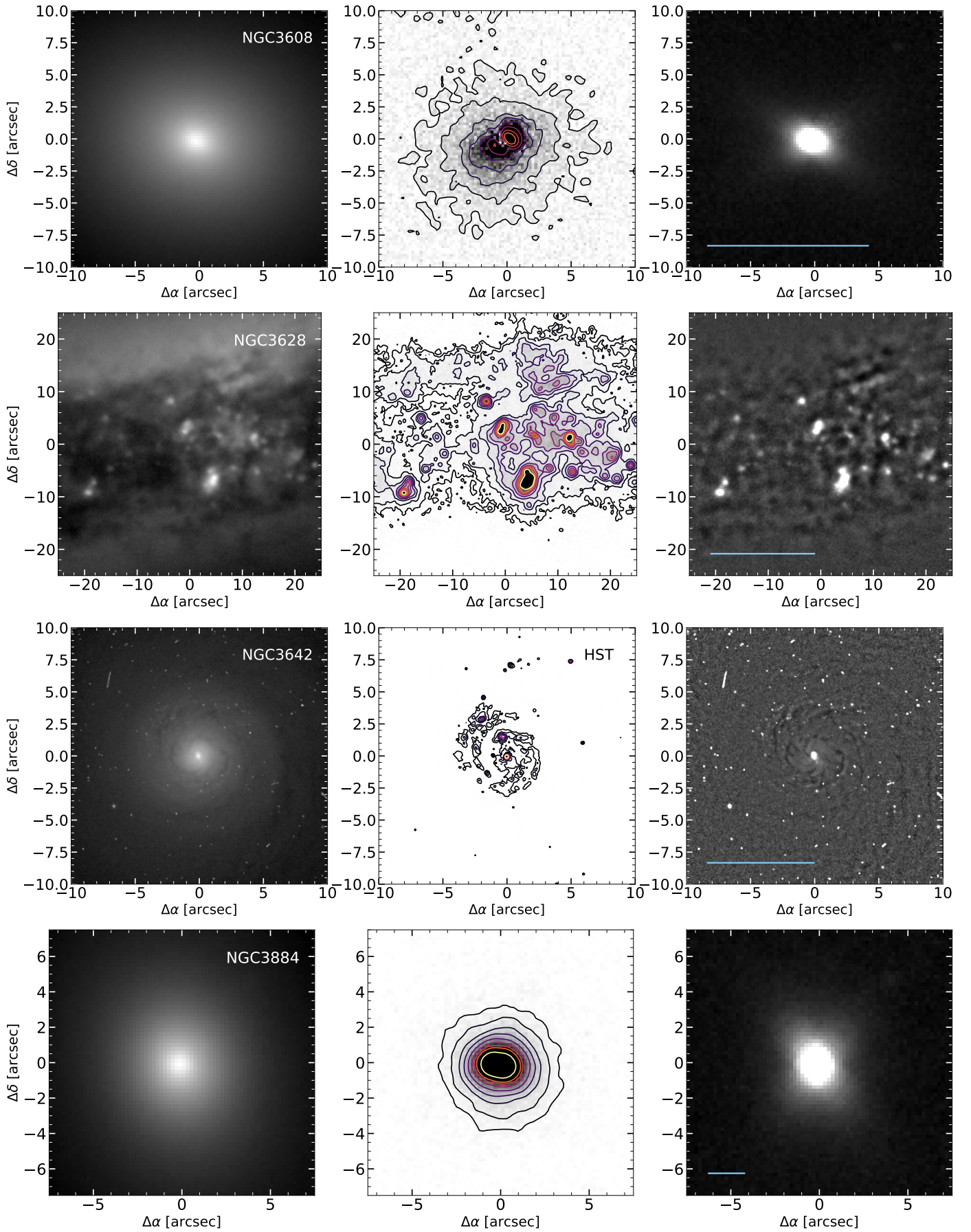


**Fig. B.3.** NGC 3608, NGC 3628, NGC 3642 and NGC 3884  $H\alpha$  emission. The complete description is in Fig. B.1.



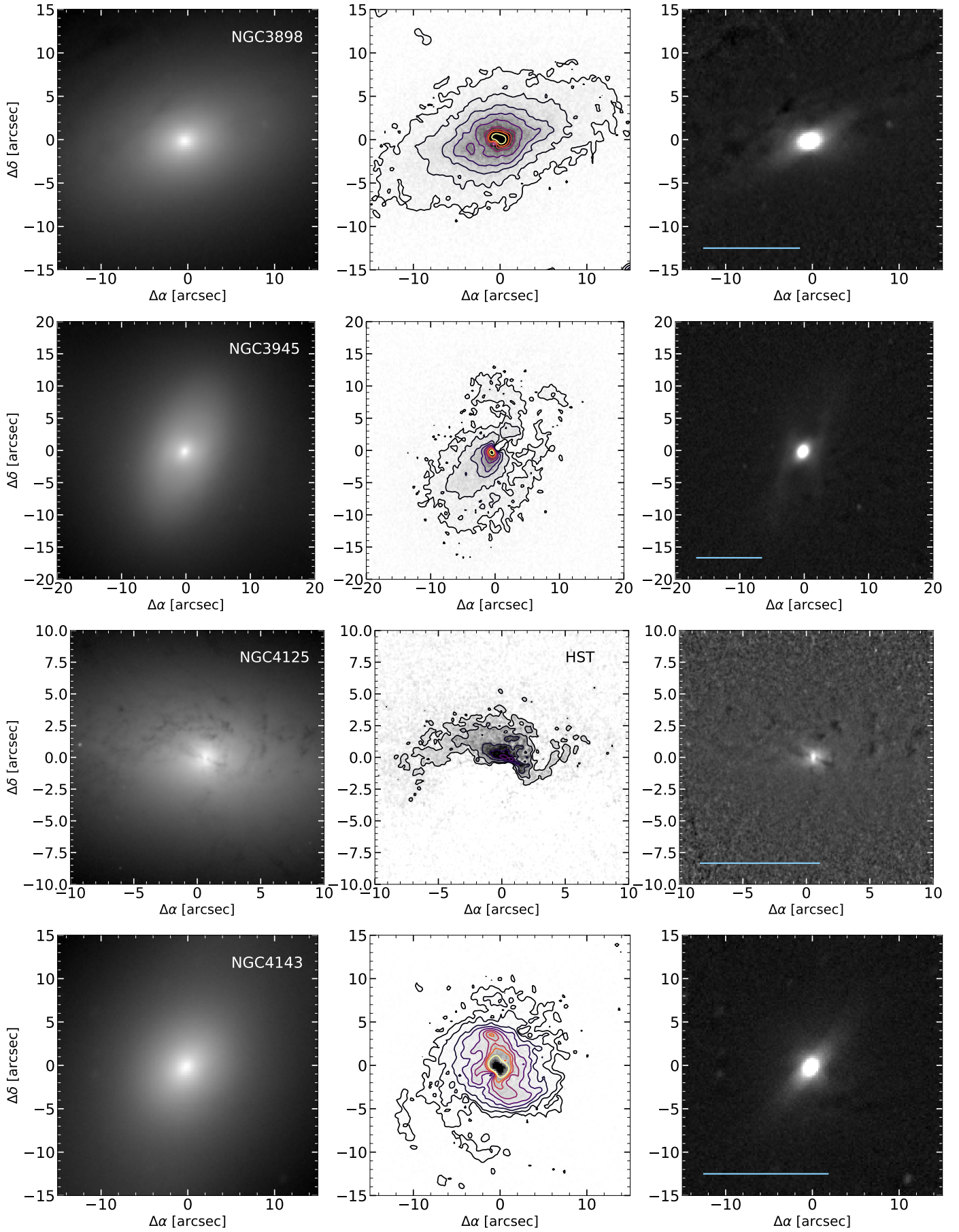


**Fig. B.4.** NGC 3898, NGC 3945, NGC 4125 and NGC 4143  $H\alpha$  emission. The complete description is in Fig. B.1.

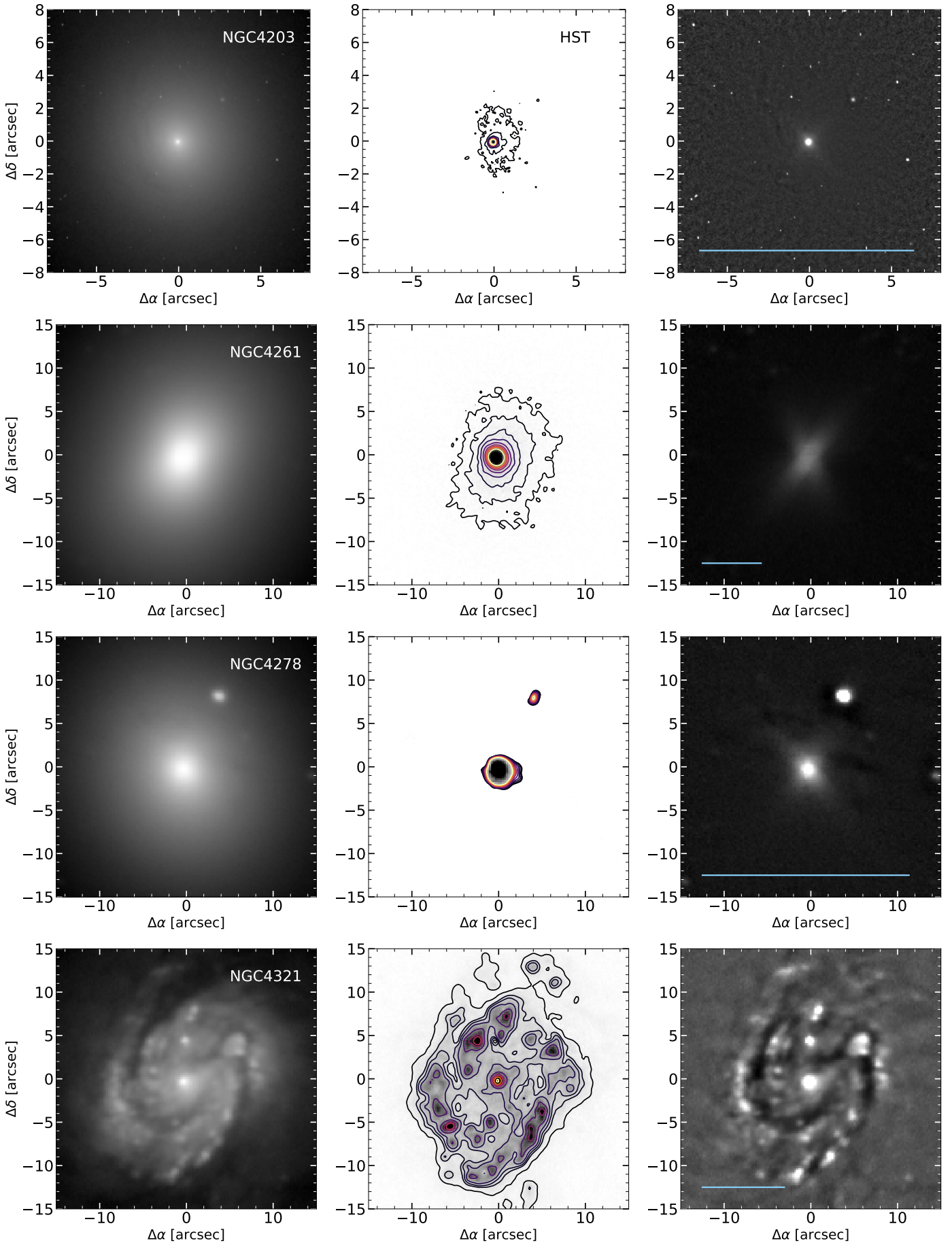


**Fig. B.5.** NGC 4203, NGC 4261, NGC 4278 and NGC 4321  $H\alpha$  emission. The complete description is in Fig. B.1.

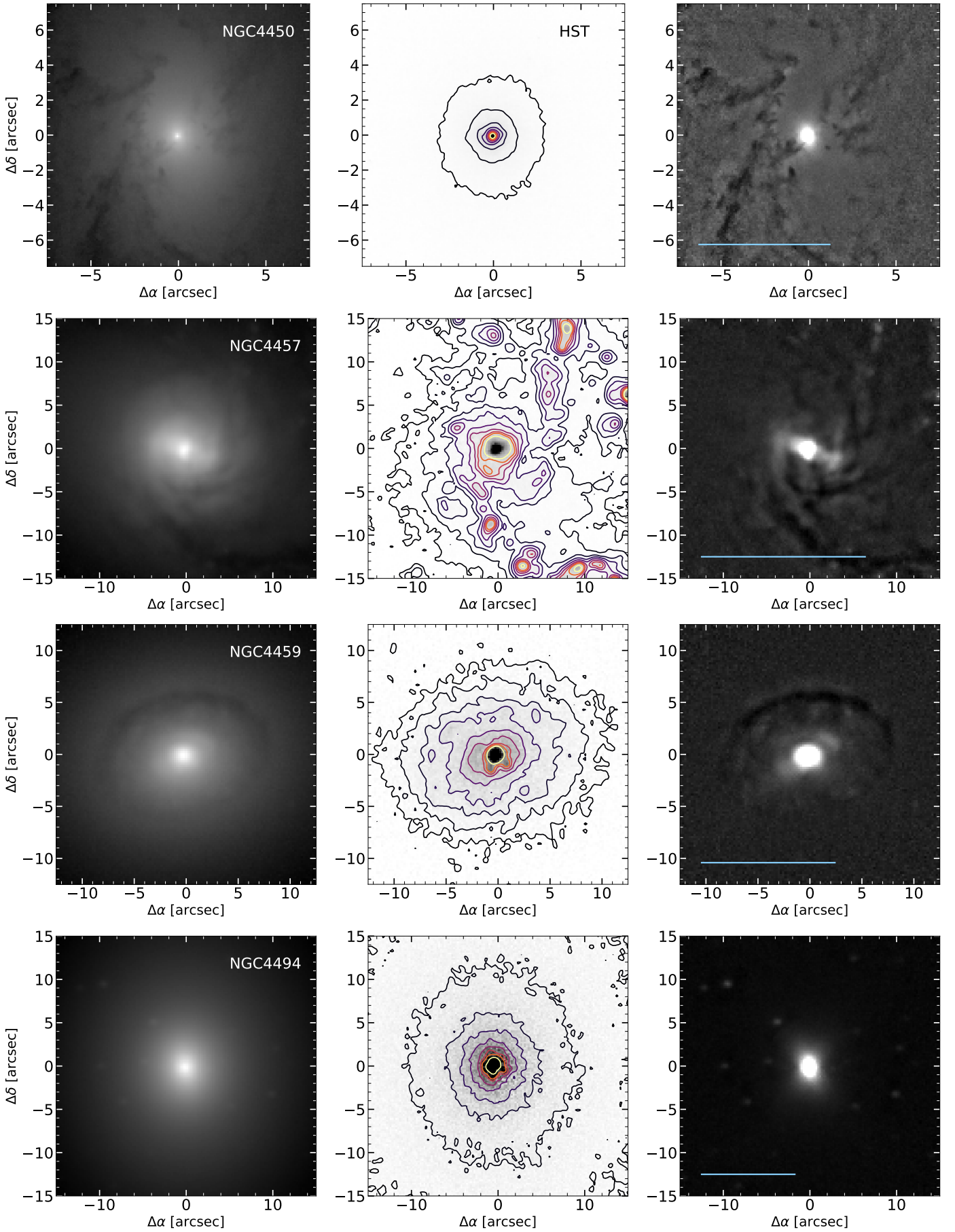


**Fig. B.6.** NGC 4450, NGC 4457, NGC 4459 and NGC 4494  $H\alpha$  emission. The complete description is in Fig. B.1.



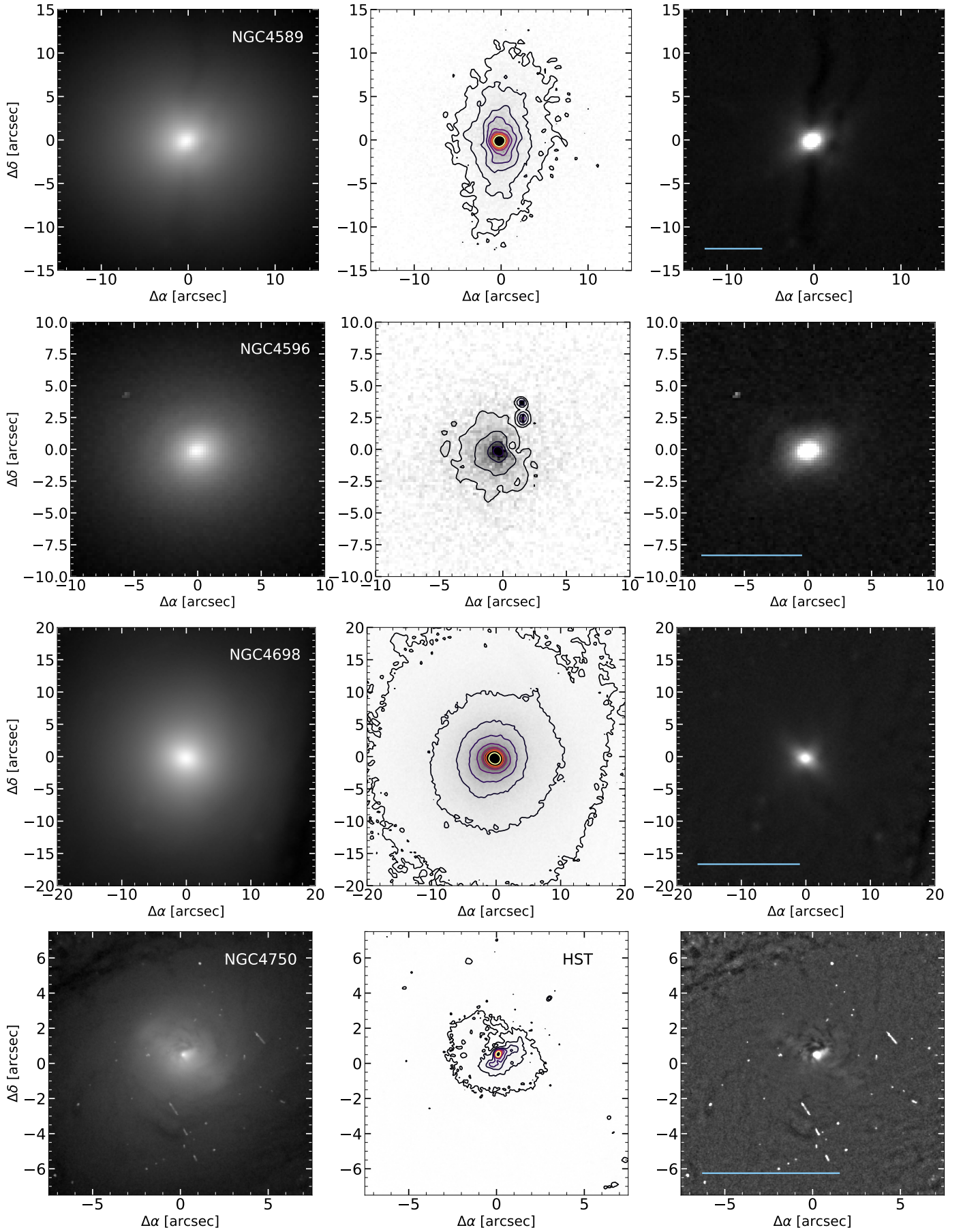


**Fig. B.7.** NGC 4589, NGC 4596, NGC 4698 and NGC 4750  $H\alpha$  emission. The complete description is in Fig. B.1.

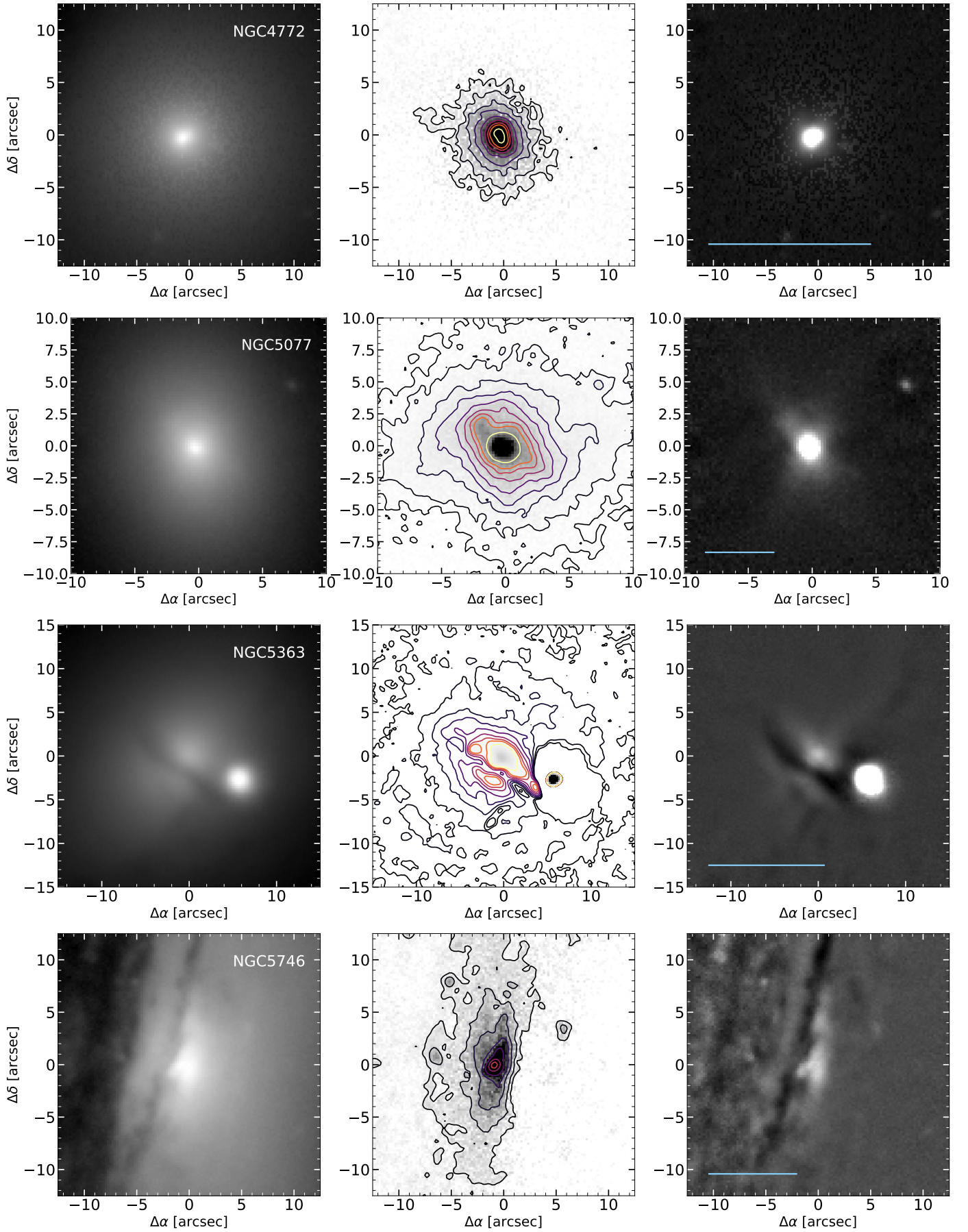


**Fig. B.8.** NGC 4772, NGC 5077, NGC 5363 and NGC 5746  $H\alpha$  emission. The complete description is in Fig. B.1.



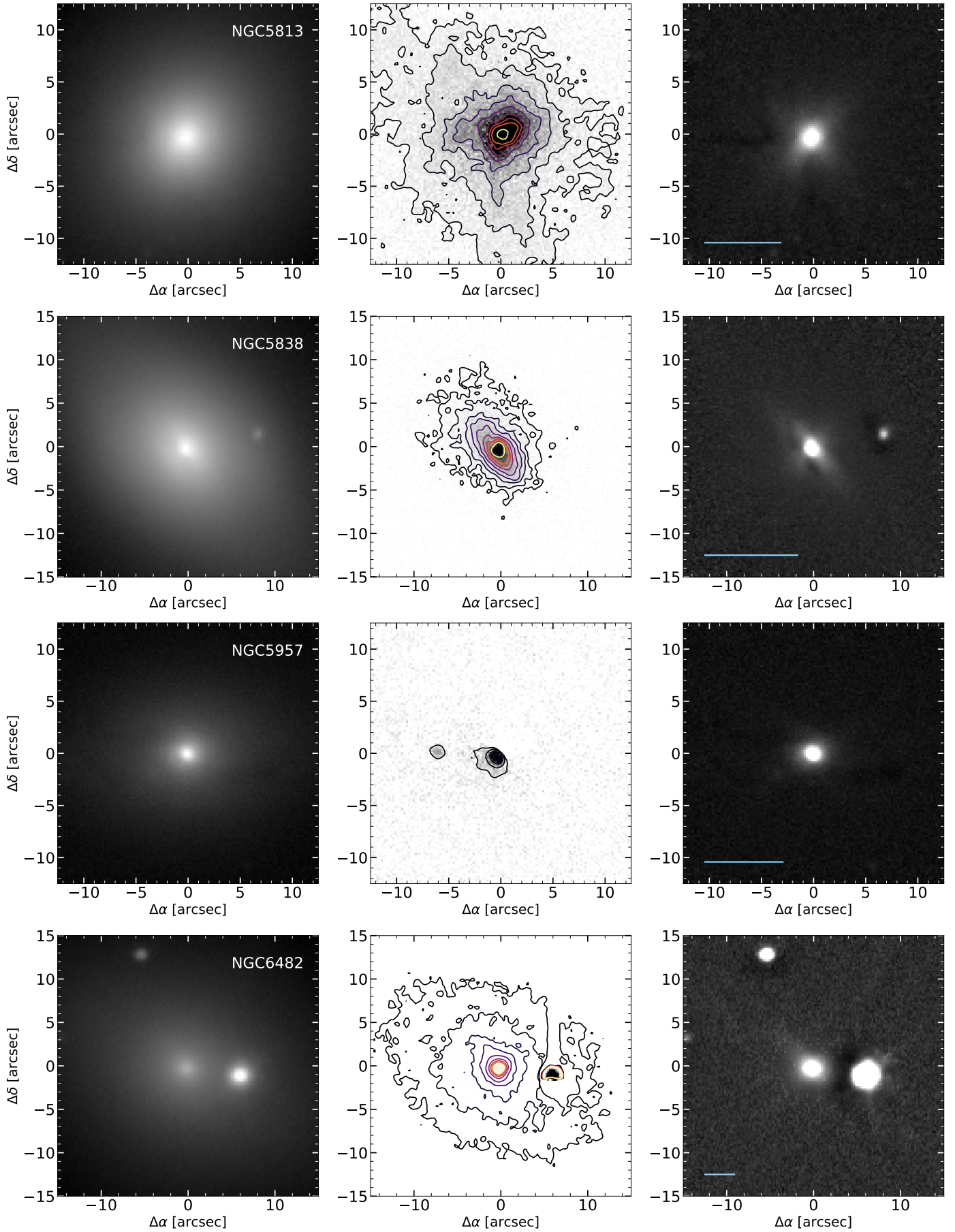


**Fig. B.9.** NGC 5813, NGC 5838, NGC 5957 and NGC 6482  $H\alpha$  emission. The complete description is in Fig. B.1.

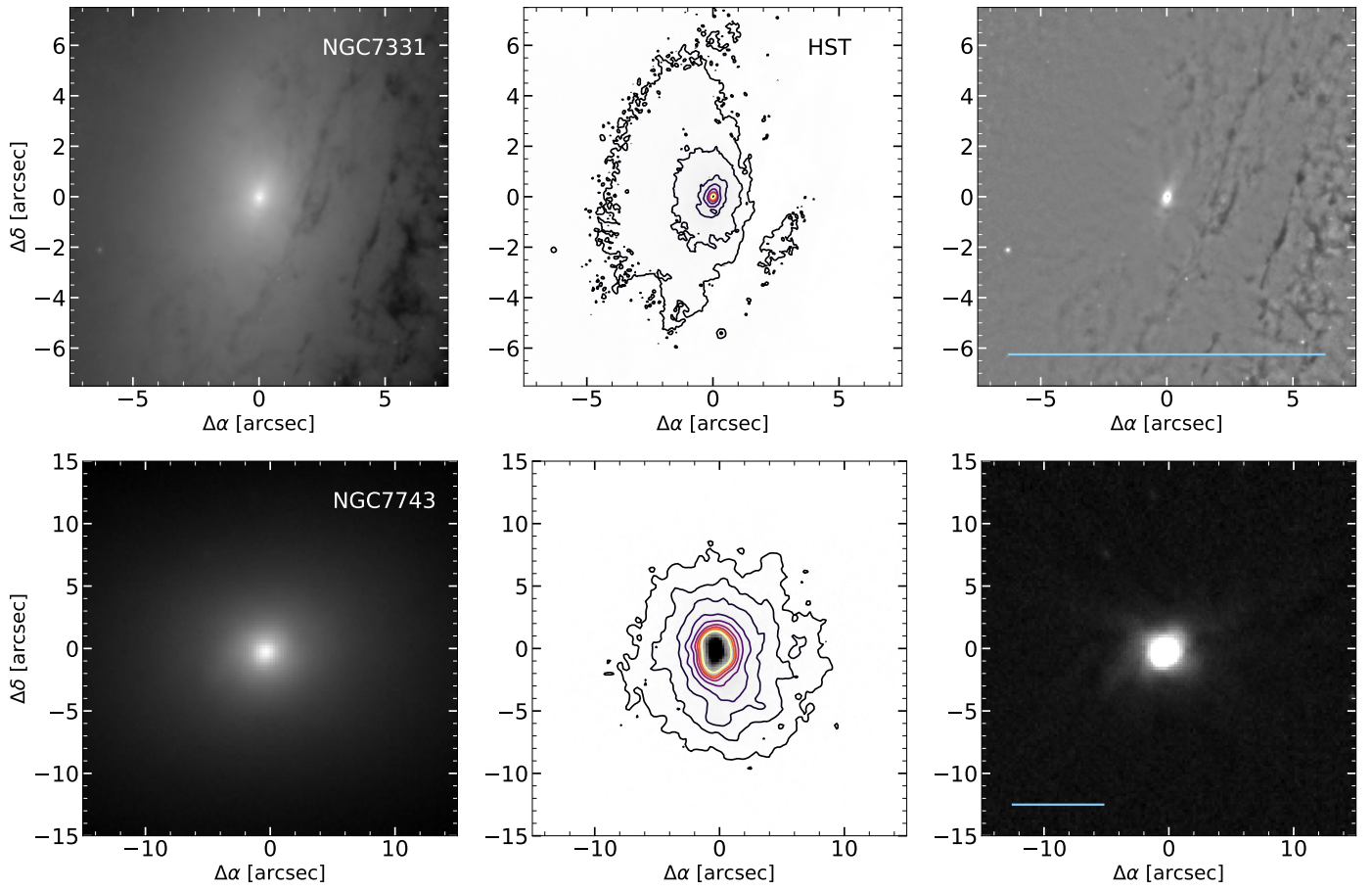


**Fig. B.10.** NGC 7331 and NGC 7743  $H\alpha$  emission. The complete description is in Fig. B.1.